Engineering Structures 282 (2023) 115835

Contents lists available at ScienceDirect

Engineering Structures

journal homepage: www.elsevier.com/locate/engstruct

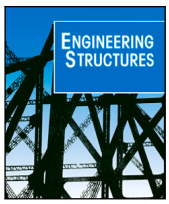

Dynamic load allowance of long-span modular steel bridges

J. Chordà-Monsonís [a,b,*], E. Moliner [b], P. Galvín [a,d], M.D. Martínez-Rodrigo [b], E. Zacchei [c,e], A. Tadeu [c,e], I. Ferraz [f], A. Romero [a]

[a] Escuela Técnica Superior de Ingeniería, Universidad de Sevilla, Camino de los Descubrimientos s/n, 41092 Sevilla, Spain
[b] Universitat Jaume I, Department of Mechanical Engineering and Construction, Avda. Sos Baynat s/n, ES-12071 Castelló, Spain
[c] ITeCons, Institute for Research and Technological Development in Construction, Energy, Environment and Sustainability, Rua Pedro Hispano s/n, 3030-289 Coimbra, Portugal
[d] ENGREEN, Laboratory of Engineering for Energy and Environmental Sustainability, Universidad de Sevilla, Camino de los Descubrimientos s/n, ES-41092, Spain
[e] Universidade de Coimbra, CERIS, Department of Civil Engineering, 3030-289 Coimbra, Portugal
[f] MBS, BERD, Edíficio Olympus, Av. D. Alfonso Henriques, 1462-2°, 4450-013, Matosinhos, Portugal

ARTICLE INFO

Keywords:
Vehicle–bridge coupled model
Road roughness
Dynamic load allowance indices
Impact factor
Finite element analysis

ABSTRACT

Modular steel bridges are structures whose construction is based on regular prefabricated truss units. This presents several advantages, such as rapid and easy deployment, high adaptability to the terrain and reduced construction costs. However, they generally face operational restrictions for span lengths greater than 60 m. Recent technological innovations search to overcome these limitations and develop modular structures with larger spans. Hence, the main objective of this work is to evaluate the dynamic effects on long-span modular steel bridges. The present contribution provides a study on two modular bridge typologies, considering different span lengths from 120 to 140 m. A 3D coupled vehicle–bridge model is used to analyse the vehicle–bridge interaction and the dynamic load allowance of the structures. The vehicle is represented as a multibody truck system and the bridges are modelled with the finite element method. Several types of randomly-generated road irregularities are considered on the bridge deck. The effect of each type of irregularity is evaluated on the dynamic load allowance of the bridges. The results obtained reveal the notable influence of road irregularities that involve abrupt vertical displacements that excite the vehicle mode shapes. In addition, it is observed that dynamic load allowance indices tend to decrease with longer spans and higher speeds, except when a resonance is produced.

1. Introduction

Since moving vehicles act as oscillators inducing forces on bridges, the dynamic interaction between both elements is one of the main concerns regarding the design, monitoring, and maintenance of the roadway bridge infrastructure. As experimental and theoretical investigations have shown, the impact of a moving vehicle on a bridge depends on many factors, including the vehicle and bridge characteristics, the speed of the vehicle and the roughness of the pavement [1]. Furthermore, the total response of the vehicle–bridge system is coupled. As a result, the complexity of the phenomenon increases and the study of the entire Vehicle–Bridge Interaction (VBI) is required to analyse the problem [2], which is a key issue in bridge engineering [3]. The dynamic effect of vehicles moving on bridges is generally evaluated with dynamic load allowance (IM) indices in many design codes [4]. Other common denominations for these indices are impact factors and dynamic amplification factors.

Modular bridges are steel truss structures constructed by means of the repetition of a prefabricated regular unit (or module) along the length of the bridge (see Fig. 1). This provides additional adaptability to the terrain, leads to a faster and easier construction process and reduces costs. Consequently, this type of bridge has been widely used as a temporary rapid erectable structure to recover damaged or destroyed communication routes [5]. Nevertheless, modular bridges are also often used as permanent structures [6].

The main limitation of modular steel bridges is attributed to the deformation caused by the combination of dynamic loads, leading to a maximum span length of 60 m, which is rarely exceeded [7]. In the case of longer spans, operational restrictions related to load capacity and circulation speed are necessary. As the effects of dynamic coupling between vehicle and bridge have become more and more significant due to the increase in operating speeds and axle loads in highway traffic [8], it is crucial to understand the dynamic behaviour of these bridges to improve their capabilities.

* Corresponding author at: Escuela Técnica Superior de Ingeniería, Universidad de Sevilla, Camino de los Descubrimientos s/n, 41092 Sevilla, Spain.
E-mail addresses: jchorda@us.es, chordaj@uji.es (J. Chordà-Monsonís).

https://doi.org/10.1016/j.engstruct.2023.115835
Received 9 November 2022; Received in revised form 30 January 2023; Accepted 16 February 2023
Available online 22 February 2023

Fig. 1. LMB-A120 bridge rendering.

Several aspects of the VBI have been extensively studied in the last decades in a variety of solutions. In this sense, Yang et al. [9] evaluated the VBI by conceiving the bridge as a simply-supported beam and the vehicle as a sprung mass. The modal superposition method was used to obtain solutions for the whole system, admitting a small vehicle to bridge mass ratio. The authors found that accurate solutions could be obtained considering only the contribution of the bridge fundamental mode. Chul et al. [10] derived the equations of motion of a three-dimensional VBI system using a variational formulation. The coupled VBI system, comprising an 8 Degree-Of-Freedom (DOF) cargo truck, a steel girder bridge and the roughness of the road was solved using Newmark's β method. Liu et al. [11] compared the response of a moving load model and a VBI model on railway bridges. The authors found that the vehicle–bridge mass and fundamental frequency ratios can determine whether the VBI effects should be taken into account. More recently, Yang et al. [12] provided a closed-form solution for calculating the dynamic response of a two-axle asymmetric vehicle moving over a bridge. The authors emphasised the utility of this approach to scan the dynamic properties of bridges. Greco et al. [13] developed a model with the Finite Element Method (FEM) consisting of a moving mesh to evaluate the VBI in presence of moving loads. The methodology was validated by comparing their results with the literature.

In the last few years, other aspects related to VBI have been studied, such as the influence of the vehicle and the bridge modal parameters on the vehicle–bridge coupled system, as in [3,14,15]; or the additional damping that the vehicle induces on the dynamic vibration of the vehicle–bridge system [16,17]. In this regard, some authors [18,19] investigated how the standards treat this matter and highlighted the complexity of the phenomenon.

As part of the excitation mechanisms of the VBI, the effect and importance of road irregularities has also been widely discussed, concluding that they can strongly affect the performance of the coupled vehicle–bridge system causing a greater dynamic response, lowering the comfort for the users and diminishing the fatigue life of bridges with poorer road conditions [20–22]. Other authors have evaluated the effect of road irregularities focusing on the dynamic load allowance. In this sense, Ma et al. [23] carried out a series of VBI analyses to assess the regularity of the IM on 15 continuous beam bridges. The authors concluded that IM indices increase dramatically when resonance occurs and also, current design codes did not take this effect into account. Deng et al. [4] developed a 3D vehicle–bridge coupled model to investigate the VBI and the IM on multi-girder concrete bridges. The authors provided additional expressions to calculate IM indices under different road conditions since they concluded that AASTHO [24] may underestimate the amplification effects on poor condition roads. Jung et al. [25] studied the IM on a total of 256 bridges and found that 32% of the structures exceeded the design criteria of the IM indices based on the span length provided in several design codes. As a result, the authors suggested a method for calculating IM indices on the basis of the natural frequency of the bridges. Mosheni et al. [26] reached similar conclusions. The authors investigated the dynamic behaviour of multicell box-girder bridges under moving loads and concluded that AASHTO [24] formulas may underestimate the IM, especially on bridges with larger spans.

The literature about the evaluation of the IM on modular steel bridges is scarce and represents a clear gap of knowledge. In one of the few publications dedicated to the matter, Montenegro et al. [27] described a stochastic methodology to evaluate IM indices considering road irregularities on two modular steel bridges. The bridges were modelled with the FEM and the vehicle as a Multibody System (MBS). The authors concluded that the technique was adequate and could lead to relevant material savings in the construction of this type of structures compared to the use of predefined IM factors proposed in the design codes. Pinkey et al. [28] used an experimental testing programme to assess the dynamic load allowance of different types of military vehicles at different speeds on a modular steel bridge. The authors found that rough bridge surfaces increase the bridge response and tracked vehicles cause less dynamic effects than wheeled ones. Other authors like Kusimba et al. [6] assessed the dynamic performance of a modular bridge and calculated its IM factor, which was well within the threshold given by AASHTO [24]. In general, for this type of bridge, other aspects are usually studied, such as damage assessment of joints and structural elements as in [29,30], or new structural construction techniques as in [5].

In view of this, the present research aims to (i) evaluate the influence of the VBI on the dynamic behaviour of long-span modular steel bridges and (ii) investigate the dynamic load allowance under different types of randomly-generated road irregularities. This represents an important novelty, because, as stated before, this is not usually the matter of research on this type of truss bridges. Furthermore, a significant part of the research effort dedicated to evaluating the IM on bridges has been focused on short-to-medium span bridges [31]. As a result, studies found in the literature generally cover significantly shorter span lengths than the ones considered in this contribution. In addition, for the sake of completeness, the effect of considering increasing span lengths is taken into account in the present paper and two different modular bridge typologies are studied to understand the dynamic effects on the structural elements of the bridges. Lastly, the separate influence of various types of randomly-generated road irregularities and their total contribution considering a wide velocity range are investigated.

To pursue the goals of the work, a 3D vehicle–bridge coupled model is implemented. The vehicle is simulated as a MBS based on the AASHTO HS20-44 truck [24]. Two bridge typologies of span lengths from 120 to 140 m for a total of six bridges are studied. The numerical models of the bridges are defined using the FEM. The VBI approach considered in this work admits that the vehicle does not significantly alter the dynamic behaviour of the bridges, and thus the modal superposition method can be applied to compute the bridge response [4,31]. The pavement of the bridges is made up of steel frames, and in this regard, the effect of three types of road irregularities is considered: (i) roughness of the pavement and (ii) bowing and (iii) misalignment of the pavement frames. The influence of the quasistatic and dynamic load contributions is analysed. Random irregularity profiles are generated on a stochastic basis from experimentally measured manufacturing imperfections. A sufficient number of simulations are carried out to ensure the representativeness of the obtained results.

This paper is organised as follows. In Section 2, the vehicle–bridge formulation is presented in detail. In Section 3, the generation of road irregularities is described. Section 4 addresses the numerical models of vehicles and bridges used in this work. In Section 5, the dynamic forces resulting from the VBI and the IM indices of the bridges under different types of irregularities are investigated. The results of the work are discussed in Section 6 and the main conclusions are derived in Section 7.

2. Vehicle–bridge coupled system

This section describes the mathematical formulation that defines the dynamic coupling between the vehicle and the bridge. The adopted procedure is based on that proposed in [32]. The vehicle is represented as a MBS and the bridges are modelled with the FEM.

2.1. Equations of motion of the vehicle

The equations of motion of the vehicle can be written as follows:

$$\mathbf{M}_v\ddot{\mathbf{u}}_v + \mathbf{C}_v\dot{\mathbf{u}}_v + \mathbf{K}_v\mathbf{u}_v = \mathbf{F}_v + \mathbf{F}_{vb} \tag{1}$$

where $\mathbf{M}_v$, $\mathbf{C}_v$ and $\mathbf{K}_v$ are the mass, damping, and stiffness matrices of the vehicle, respectively, and $\mathbf{u}_v$ is its displacement vector. A dot over a variable denotes the time derivative. The right-hand side of the equation represents the force vector caused by the effect of gravity $\mathbf{F}_v$ and the interaction force $\mathbf{F}_{vb}$ at the contact points between the vehicle and the bridge.

2.2. Equations of motion of the bridge

The equilibrium equation of the bridge can be written as follows:

$$\mathbf{M}_b\ddot{\mathbf{u}}_b + \mathbf{C}_b\dot{\mathbf{u}}_b + \mathbf{K}_b\mathbf{u}_b = \mathbf{F}_b + \mathbf{F}_{bv}\,, \tag{2}$$

where $\mathbf{M}_b$, $\mathbf{C}_b$ and $\mathbf{K}_b$ are the mass, damping, and stiffness matrices, respectively. $\mathbf{u}_b$ is the displacement vector of the bridge and $\mathbf{F}_b$ represents the forces applied to it. The interaction force $\mathbf{F}_{bv}$ is defined at the contact points as well. The displacement vector can be expressed in modal coordinates as:

$$\mathbf{u}_b(\mathbf{x},t) = \sum_{j=1}^{m}\phi_j(\mathbf{x})Y_j(t) = \boldsymbol{\Phi}(\mathbf{x})\mathbf{Y}(t)\,, \tag{3}$$

where $\phi_j(x)$ and $Y_j(t)$ are the j-th modal shape and generalised coordinate, respectively. Then, the projection of Eq. (2) in the modal space of dimension m gives the subsequent modal equations, admitting a viscous modal damping approach:

$$\mathbf{I}\ddot{\mathbf{Y}} + \mathbf{Z}\dot{\mathbf{Y}} + \boldsymbol{\Omega}\mathbf{Y} = \boldsymbol{\Phi}^T(\mathbf{F}_{bv} + \mathbf{F}_b) \tag{4}$$

$$\mathbf{I} = \begin{bmatrix} \ddots & & \\ & 1 & \\ & & \ddots \end{bmatrix}_{m\times m}, \quad \mathbf{Z} = \begin{bmatrix} \ddots & & \\ & 2\zeta_j\omega_j & \\ & & \ddots \end{bmatrix}_{m\times m}, \quad \boldsymbol{\Omega} = \begin{bmatrix} \ddots & & \\ & \omega_j^2 & \\ & & \ddots \end{bmatrix}_{m\times m}. \tag{5}$$

where ω_j is the j-th natural frequency and ζ_j is the j-th corresponding modal damping.

2.3. Vehicle–bridge interaction

The vehicle–bridge interaction force in the ith wheel is defined as:

$$\mathbf{F}_{vbi} = k_{wi}\Delta_i + c_{wi}\dot{\Delta}_i \tag{6}$$

where k_{wi} and c_{wi} represent the stiffness and damping of the tyres, and Δ_i and $\dot{\Delta}_i$ are the relative vertical displacement and velocity between the i-th wheel and the bridge deck at the contact point:

$$\Delta_i = \mathbf{u}_{vi} - (R_i + \mathbf{u}_{bi}) \tag{7a}$$

$$\dot{\Delta}_i = \dot{\mathbf{u}}_{vi} - (\dot{R}_i + \dot{\mathbf{u}}_{bi}) \tag{7b}$$

In these equations, $\mathbf{u}_{vi}$ is the vertical displacement of the i-th wheel of the vehicle. $\mathbf{u}_{bi}$ and R_i represent the vertical displacement of the bridge and the total irregularity profile of the road surface under the i-th wheel, respectively. Fig. 2 shows a scheme of the relative displacement components of the system.

The displacement of the bridge at the contact point i is computed using finite elements as:

$$\mathbf{u}_{bi} = \sum_{k=1}^{p} N_k\mathbf{u}_{bk}^e = \mathbf{N}\mathbf{u}_b^e \tag{8}$$

where p is the number of nodes, e is the element to which the i-th contact point belongs, N_k represents the element shape functions and $\mathbf{u}_{bk}^e$ are the nodal displacements. The force component related to the bridge velocity in Eq. (6) is approximated according to:

$$\begin{aligned}\dot{\mathbf{u}}_{bi} + \dot{R}_i &= \frac{d\mathbf{N}}{dx}\frac{dx}{dt}\mathbf{u}_b^e + \mathbf{N}\frac{d\mathbf{u}_b^e}{dt} + \frac{dR_i}{dx}\frac{dx}{dt} \\ &= \mathbf{N}_{,x}v\mathbf{u}_b^e + \mathbf{N}\dot{\mathbf{u}}_b^e + R_{i,x}v\end{aligned} \tag{9}$$

where v, here assumed constant, represents the passing velocity of the vehicle. Then, introducing Eqs. (3), (8) and (9) in Eq. (6), the vehicle–bridge interaction force at the contact point i can be expressed as:

$$\begin{aligned}\mathbf{F}_{vbi} &= k_{wi}(\mathbf{u}_{vi} - (R_i + \mathbf{N}\mathbf{u}_b)) + c_{wi}(\dot{\mathbf{u}}_{vi} - (\mathbf{N}_{,x}v\mathbf{u}_b^e + \mathbf{N}\dot{\mathbf{u}}_b^e + R_{i,x}v)) \\ &= k_{wi}(\mathbf{u}_{vi} - (R_i + \mathbf{N}\boldsymbol{\Phi}\mathbf{Y})) + c_{wi}(\dot{\mathbf{u}}_{vi} - (\mathbf{N}_{,x}v\boldsymbol{\Phi}\mathbf{Y} + \mathbf{N}\boldsymbol{\Phi}\dot{\mathbf{Y}} + R_{i,x}v))\end{aligned} \tag{10}$$

Furthermore, the interaction force in the structure is obtained from the total number of vehicle tyres w according to the following expression:

$$\mathbf{F}_{bv} = \sum_{i=1}^{w}\mathbf{N}_i^T\mathbf{F}_{bvi} = -\sum_{i=1}^{w}\mathbf{N}_i^T\mathbf{F}_{vbi} \tag{11}$$

where the transposed shape function matrix $\mathbf{N}_i^T$ is evaluated on the i-th wheel. Once the interaction force is known, it is possible to define an equation of motion to represent the dynamic behaviour of the coupled vehicle–bridge system. The equilibrium equation of the bridge defined in Eq. (4) considering the interaction force of each wheel becomes:

$$\begin{aligned}&\mathbf{I}\ddot{\mathbf{Y}} + \left(\mathbf{Z} + \boldsymbol{\Phi}^T\left(\sum_{i=1}^{w}\mathbf{N}_i^T c_{wi}\mathbf{N}_i\right)\boldsymbol{\Phi}\right)\dot{\mathbf{Y}} \\ &+ \left(\boldsymbol{\Omega} + \boldsymbol{\Phi}^T\left(\sum_{i=1}^{w}\mathbf{N}_i^T\left(k_{wi}\mathbf{N}_i + c_{wi}v\mathbf{N}_{i,x}\right)\right)\boldsymbol{\Phi}\right)\mathbf{Y} = \\ &- \boldsymbol{\Phi}^T\sum_{i=1}^{w}\mathbf{N}_i^T(k_{wi}(\mathbf{u}_{vi} - R_i) + c_{wi}(\dot{\mathbf{u}}_{vi} - R_{i,x}v))\end{aligned} \tag{12}$$

Then, the equation of motion of the vehicle in Eq. (1) and the interaction force in Eq. (10) allow the following:

$$\begin{aligned}\mathbf{M}_v\ddot{\mathbf{u}}_v + \mathbf{C}_v\dot{\mathbf{u}}_v + \mathbf{K}_v\mathbf{u}_v = \mathbf{F}_v + \sum_{i=1}^{w}\big[&k_{wi}(\mathbf{u}_{vi} - (R_i + \mathbf{N}_i\boldsymbol{\Phi}\mathbf{Y})) \\ &+ c_{wi}(\dot{\mathbf{u}}_{vi} - (\mathbf{N}_{i,x}v\boldsymbol{\Phi}\mathbf{Y} + \mathbf{N}_i\boldsymbol{\Phi}\dot{\mathbf{Y}} + R_{i,x}v))\big]\end{aligned} \tag{13}$$

Eqs. (12) and (13) are written in a coupled system of equations that permits the calculation of the displacements of the bridge and the vehicle. The system matrices vary each time step according to the vehicle position. Then, an explicit Runge–Kutta time marching scheme [33,34] is adopted to solve the VBI problem.

3. Generation of road irregularities

In this study, three types of road irregularities are considered: (i) roughness of the pavement surface, (ii) bow defects of the pavement frames due to manufacturing imperfections and (iii) misalignment of the pavement frames due to faulty installation. In the following, the mathematical representation of these irregularity types is explained.

First, the pavement roughness is defined as a stationary stochastic process based on a Power Spectral Density function (PSD) as per ISO-8608 [35]. The irregularity profile $r(x)$ is given by a zero-mean normal stationary ergodic random process described by its PSD function $S(\kappa)$:

$$S(\kappa_n) = S(\kappa_0)\left(\frac{\kappa_n}{\kappa_0}\right)^{-2} \tag{14}$$

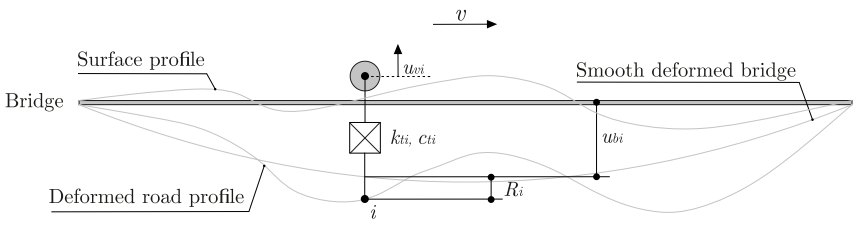

Fig. 2. Relative displacement components between the vehicle and the bridge.

where κ_n is the spatial frequency and $S(\kappa_0)$ is the one-sided PSD for the reference spatial frequency κ_0. The PSD reference value depends on the road condition and is defined in ISO-8608 [35] for different road classes. Then, the irregularity profile is calculated as the sum of a series of harmonics, as:

$$r(x) = \sum_{n=0}^{N_s} \sqrt{2\, S(\kappa_n)\Delta\kappa}\cos(2\pi\,\kappa_n x + \varphi_n) \tag{15}$$

where φ_n is the random phase angle uniformly distributed in the interval $[0, 2\pi]$, N_s is the total number of samples and $\Delta\kappa$ is the incremental κ to compute the irregularity profile.

Second, the irregularity of the pavement bowing corresponds to imperfections in the pavement frames in the form of bow defects. The bowing displacement b_q in the centre of the q-th frame is calculated on the basis of the relative deflection in the centre of a simply supported beam subjected to a uniformly distributed load:

$$b_q(x_q) = B_q \frac{-384\, x_q}{120\, L_p^4}(L_p^3 - 2L_p x_q^2 + x_q^3) \tag{16}$$

where the local coordinate $x_q = x - L_p(q-1)$ represents the position of the contact point of the vehicle within the length of the pavement frame L_p. On the other hand, the amplitude of b_q is ranged by the random parameter B_q, which is defined as a normal distribution:

$$B_q \sim N(\mu_B, \sigma_B) \tag{17}$$

where μ_B and σ_B are the mean and standard deviation of the distribution, respectively. In a similar way, the misalignment irregularity is defined as a vertical step defect in the transverse joints of the pavement frames. The amplitude of this defect M_q is defined as:

$$M_q \sim N(\mu_M, \sigma_M) \tag{18}$$

where μ_M and σ_M are the mean and standard deviation of the normal distribution.

The total unevenness at the bridge coordinate x is calculated as the combination of these three types of irregularities:

$$R(x) = r(x) + \sum_{q=1}^{Q}(b_q + M_q)[H(x - L_p(q-1)) - H(x - L_p q)] \tag{19}$$

where Q is the total number of pavement frames and H represents the Heaviside step function referred to the q-th frame.

4. Evaluation of dynamic load allowance

This section explains the adopted approach to investigate the dynamic load allowance of modular bridges. Sections 4.1 and 4.2 address the truck and the bridges considered for the study, respectively. Then, the configuration of the road irregularities considered in the analyses is detailed in Section 4.3.

4.1. The HS20-44 truck

The vehicle used in this work is based on the HS20-44 truck included in the AASHTO specifications [24]. As can be seen in Fig. 3, the truck is represented as a 3D MBS which considers the mass and inertia of the axles, front and rear truck bodies, and the stiffness and damping of the suspensions. Tyres and suspensions are modelled as linear elastic springs and dampers. Subscripts f, m and r indicate front, middle and rear, and subscripts v, s, a and w stand for vehicle, suspensions, axles, and tyres, respectively. The total load from front to rear axles is $P = [35.2, 142.4, 142.4]$ kN. Three degrees of freedom are assigned to both car bodies: u_v indicates vertical displacement, θ_v corresponds to rotation about the transverse axis (or pitching) and ϕ_v represents rotation about the longitudinal axis (or rolling). The axles are rigid and have two DOFs assigned: u_a and ϕ_a. Furthermore, the DOF corresponding to the vertical displacement of each wheel is also taken into account. In total, 18 DOFs are considered to represent the vehicle behaviour. The parameters of the complete truck model are adopted from Refs. [4,20] and listed in Table 1.

Table 1
Parameters of the HS20-44 truck. Note that the abbreviation COM stands for Center Of Mass.

Parameter	Description	Value	Unit
m_{v1}	Mass of truck body 1	2612	kg
$I_{\theta v1}$	Pitching moment of inertia of truck body 1	2022	kg m^2
$I_{\phi v1}$	Rolling moment of inertia of truck body 1	8544	kg m^2
m_{v2}	Mass of truck body 2	26113	kg
$I_{\theta v2}$	Pitching moment of inertia of truck body 2	33153	kg m^2
$I_{\phi v1}$	Rolling moment of inertia of truck body 2	181216	kg m^2
m_{a1}	Mass of the first axle suspension	490	kg
$I_{\phi a1}$	Rolling moment of inertia of first axle suspension	350	kg m^2
k_{sf}	Upper spring stiffness of the first axle	242604	N/m
c_{sf}	Upper damper coefficient of the first axle	2190	Ns/m
k_{wf}	Lower spring stiffness of the first axle	875082	N/m
c_{wf}	Lower damper coefficient of the first axle	2000	Ns/m
m_{a2}	Mass of the second axle suspension	808	kg
$I_{\phi a2}$	Rolling moment of inertia of second axle suspension	600	kg m^2
k_{sm}	Upper spring stiffness of the second axle	1903172	N/m
c_{sm}	Upper damper coefficient of the second axle	7882	Ns/m
k_{wm}	Lower spring stiffness of the second axle	3503307	N/m
c_{wm}	Lower damper coefficient of the second axle	2000	Ns/m
m_{a3}	Mass of the third axle suspension	653	kg
$I_{\phi a3}$	Rolling moment of inertia of third axle suspension	600	kg m^2
k_{sr}	Upper spring stiffness of the third axle	1969034	N/m
c_{sr}	Upper damper coefficient of the third axle	7182	Ns/m
k_{wr}	Lower spring stiffness of the third axle	3507429	N/m
c_{wr}	Lower damper coefficient of the third axle	2000	Ns/m
L_1	Length from first axle to COM of truck body 1	1.698	m
L_2	Length from second axle to COM of truck body 1	2.569	m
L_3	Length from second axle to COM of truck body 2	1.984	m
L_4	Length from third axle to COM of truck body 2	2.283	m
L_5	Length from COM of truck body 1 to pivot joint	2.215	m
L_6	Length from COM of truck body 2 to pivot joint	2.238	m
b	Half width of the truck	1.1	m

The main mode shapes of the vehicle are represented in Fig. 4. The first one corresponds to the rolling of the rear axle and the rear truck body. The second mode involves the vertical displacement of the three axles and the pitching of the front and rear truck bodies with opposite rotations. Similarly, the third mode consists of the vertical displacement of the axles and the pitching of both truck bodies. The fourth mode corresponds to the rolling of the front and middle axles and the front truck body. The fifth and sixth modes involve higher displacements of the axles and the pitch of front and rear truck bodies.

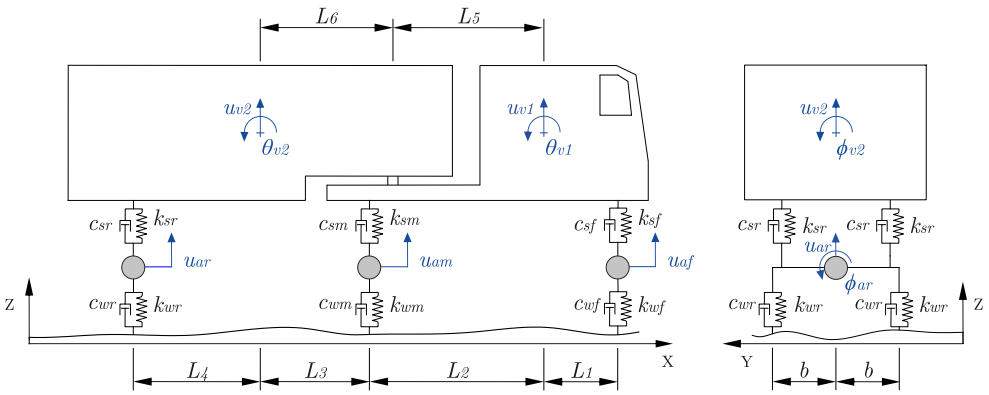

Fig. 3. HS20-44 vehicle model [24].

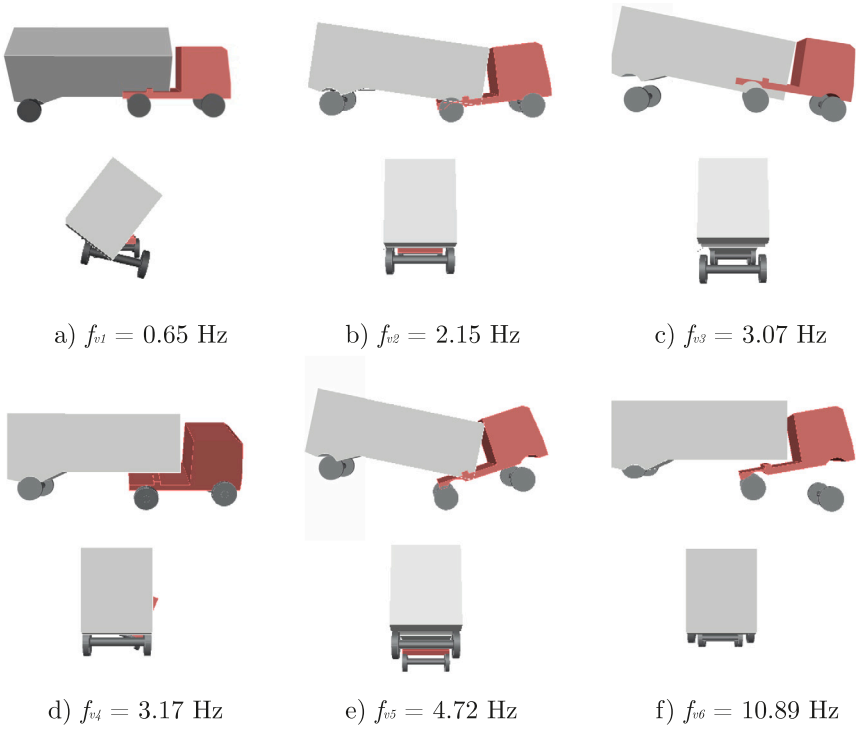

Fig. 4. Mode shapes of the HS20-44 truck.

4.2. Long-span modular bridges under study

In this contribution, the dynamic allowance of two Long-span Modular Bridges (LMBs) is investigated. The bridges under study are part of a developing project of the bridge design company BERD [36]. In particular, two different modular typologies with three different span lengths in each case are considered. The first typology, designated as LMB-R, corresponds to a modular truss bridge that includes a number of reinforced modules at both ends of the structure. The reinforced modules present the same spatial distribution as the other modules, but are composed of different structural elements in order to resist higher loads close to the supports. The second bridge typology, designated as LMB-A, is composed of structurally identical modules. In addition, an arch is built on top of the modules along the span of the bridge.

Fig. 5 shows three images of the LMB-R bridges. For this typology, three different bridges with different span lengths approaching 120, 130 and 140 m are considered. In the following, these bridges are referred to as LMB-R120, LMB-R130 and LMB-R140. In all cases, the bridges are simply-supported, and six reinforced modules are considered in total: three at each end of the bridge, as can be seen in Fig. 5(a). Each module consists of a three-dimensional truss. Modules are connected through bolted connections in the chords and in the posts. In the inferior part, each truss is connected by means of three floor crossbeams, two horizontal and two longitudinal bracings to provide the necessary stability between modules. At the top of the module, the truss connection is carried out by lateral bracings. The lower chords are connected to the upper chords by means of posts and diagonals. The length, width and height of each module are represented as L_m, W_m, and H_m, respectively. The length of the end truss is denoted as L_{end}.

Details of the LMB-A typology are shown in Fig. 6. In the same way as in the previous case, three simply-supported bridges are defined for this typology, approaching 120, 130 and 140 m of span length. These bridges are designated as LMB-A120, LMB-A130 and LMB-A140, respectively. In this case, the modules form a more complex three-dimensional structure that includes an arch of height H_a that extends throughout the length of the bridge. Each side of the module is formed

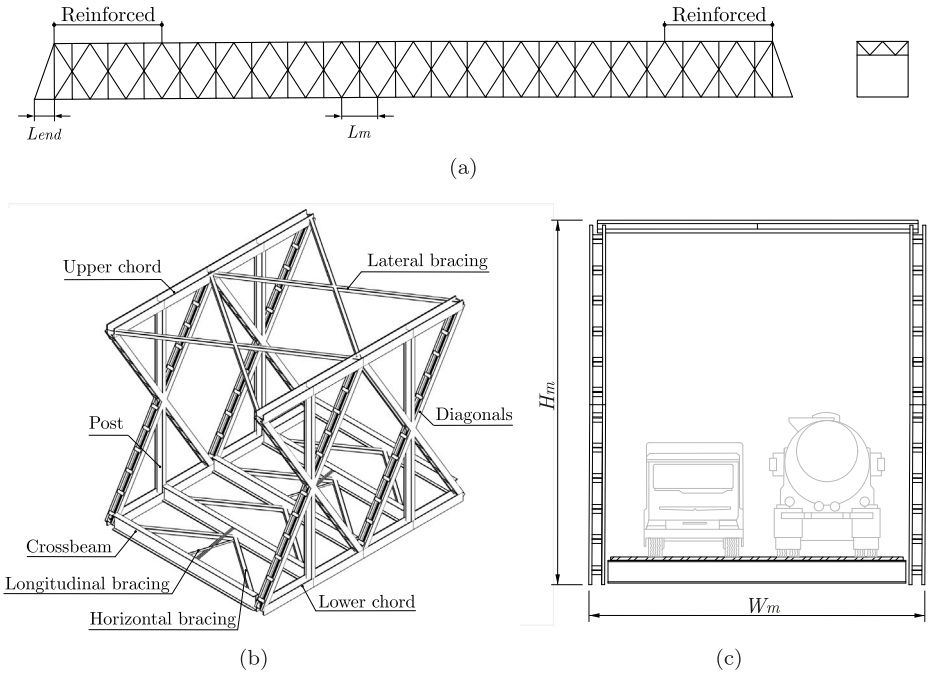

Fig. 5. LMB-R bridge typology. (a): schematic front and side view, (b): isometric view of two modules, and (c): module cross-section.

Table 2
General properties of the LMB-R and LMB-A bridges.

Bridges	M	L_m [m]	L_{end} [m]	L_b [m]	W_m [m]	H_m [m]	m_b [kg]	f_{b1} [Hz]
LMB-R120	19	6	3	120	9	10	5.843×10^5	1.48
LMB-R130	21	6	3	132	9	10	6.580×10^5	1.23
LMB-R140	23	6	3	144	9	10	7.345×10^5	1.04
LMB-A120	20	5.6	2.8	117.6	11.5	8.3	9.992×10^5	1.39
LMB-A130	22	5.6	2.8	128.8	11.5	8.3	1.100×10^6	1.17
LMB-A140	24	5.6	2.8	140	11.5	8.3	1.211×10^6	0.99

Table 3
Normalised steel profiles for the main structural elements of the LMB-R and LMB-A bridges.

Element	LMB-R (Standard modules)	LMB-R (Reinforced modules)	LMB-A
Arch	–	–	2 HEA 300
Upper posts	–	–	IPE 300
Upper chords	450 × 35-450 × 15	450 × 25-450 × 12	HEA 300
Posts	IPE 450	IPE 450	IPE 500
Diagonals	2 UPN 220	2 UPN 260	SHS 180 × 5
Lower chords	450 × 30-450 × 15	450 × 20-450 × 12	HEA 400

by a double truss that comprises lower, upper chords and diagonals. These elements are linked by the lower posts. The bottom connection between modules is provided by three floor cross-beams and two horizontal bracings. At the top of the module, four lateral bracings and a strut attach both trusses. The arch is connected to the modules by means of the upper posts and two sway bracings that join at the centre of the strut.

The bridge deck is composed of light pavement steel frames of length $L_p = 2.8\,\text{m}$. The equivalent density and thickness of the pavement frames is set as $\rho_p = 753\,\text{kg/m}^3$ and $h_p = 0.072\,\text{m}$ on the basis of experimental measurements.

The main properties of the bridges are listed in Table 2, where M indicates the number of modules, L_b is the length of the bridge, m_b is the total mass and f_{b1} is the fundamental frequency, which corresponds to the first longitudinal bending mode of the bridges. In the case of the LMB-A typology, H_m refers to the height of the module without considering the arch. The maximum height of the arch H_a is reached at mid-span and is equal to 7 m.

Fig. 7 shows the FEM of the LMB-R120 and LMB-A120 bridges. The bridge is modelled using beam elements based on the Timoshenko formulation and shell elements to represent the pavement frames. The normalised steel profiles of the main structural elements of the bridges (see Figs. 5(b) and 6(b)) are listed in Table 3. For the LMB-R bridges, standard and reinforced modules are differentiated.

The first three longitudinal bending modes of the LMB-R120 and LMB-A 120 bridges are shown in Fig. 8. These mode shapes are representative of the other bridge lengths considered in each typology.

4.3. Road irregularities

The road unevenness considered in the dynamic analyses includes five different irregularity cases. First, the quasistatic excitation mechanism is considered. In this case, the dynamic problem is solved by only taking into account the self-weight of the vehicle, and no irregularities are considered. Then, three irregularity cases are defined on the basis of the unevenness types detailed in Section 3: the pavement roughness, bowing and misalignment.

The pavement roughness is defined according to ISO-8608 [35], where the degree of unevenness is determined on the basis of the road surface condition, varying from road class A (very good) to road class E (very poor). However, this classification is provided for asphalt roads, which are more prone to exhibit important defects. In this study, the bridge pavement consists of a 1 mm thick coating that acts as a protective layer of the steel frames, and the maximum roughness amplitude of this layer is expected to be equal to its thickness in the worst-case scenario. Thus, a value of $S(\kappa_0) = 0.35 \times 10^{-6}\,\text{m}^3/\text{rad}$ is adopted with a reference spatial frequency of $\kappa_0 = 0.1\,\text{m}^{-1}$. The $\Delta\kappa$ increment and the number of spatial frequency samples are set to $\Delta\kappa = 4.5 \times 10^{-5}\,\text{m}^{-1}$ and $N_s = 2000$.

Table 4 summarises the irregularity parameters. The first column indicates if the effect of gravity is considered in the dynamic analyses, while S_n is the number of simulations performed in each case per vehicle speed. To define the bowing and misalignment irregularities, a

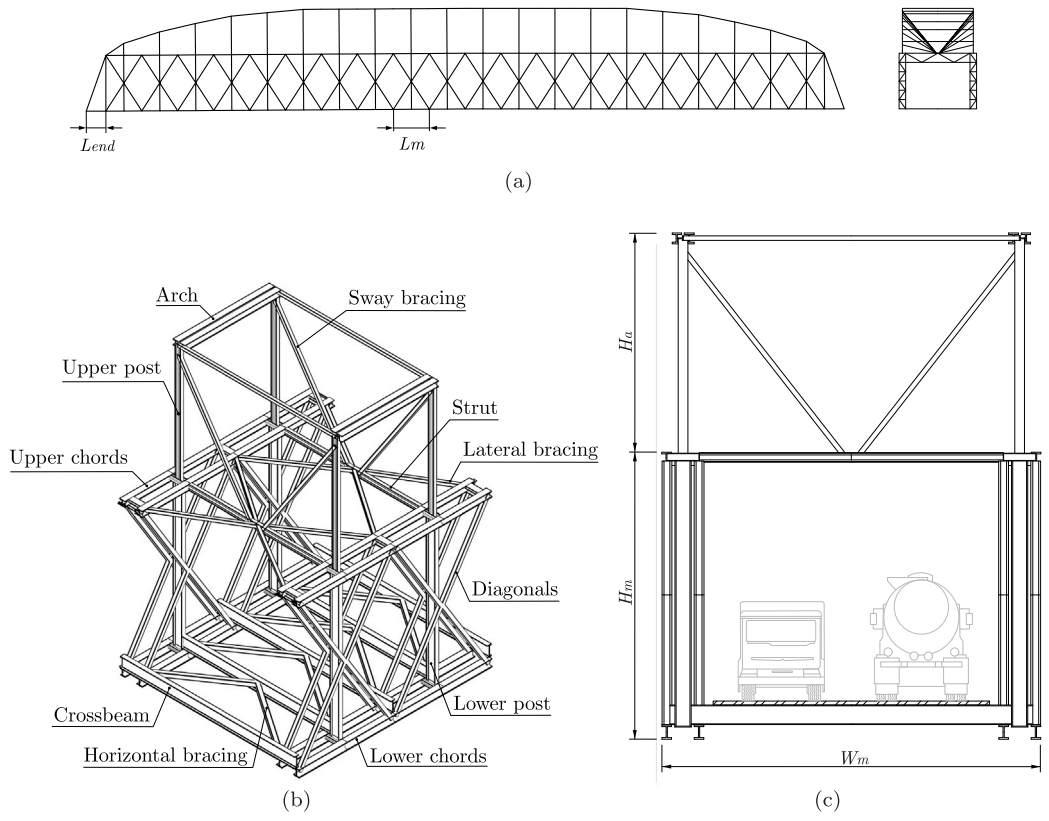

Fig. 6. LMB-A bridge typology. (a): schematic front and side view, (b): isometric view of two modules, and (c): module cross-section.

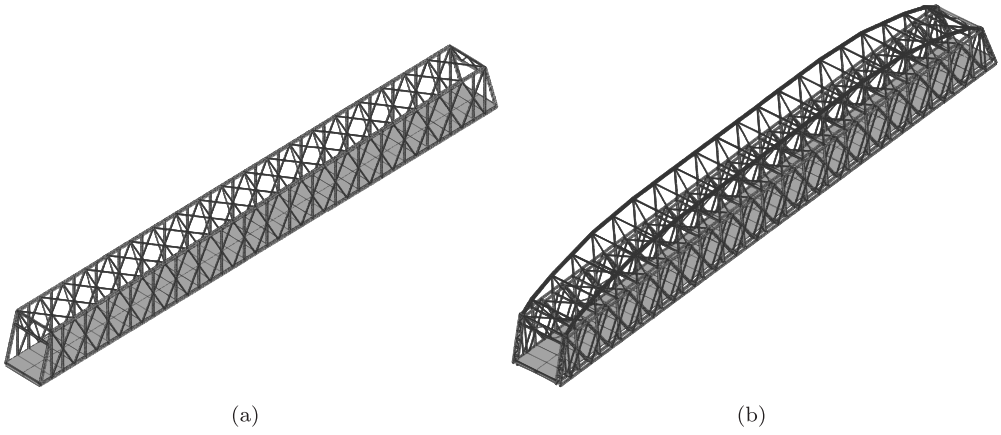

Fig. 7. View of the FEMs of the bridges. (a): LMB-R120 bridge, and (b): LMB-A120 bridge.

Table 4
Configuration and main parameters that define the five irregularity cases.

Irregularity case	Gravity	S_n	Parameters
Quasistatic	Yes	1	–
Pavement roughness	No	256	$S(k_0) = 0.35 \times 10^{-6}\,\mathrm{m}^3/\mathrm{rad}$
Pavement bowing	No	256	$\mu_B = 2.3296\,\mathrm{mm}$, $\sigma_B = 1.0738\,\mathrm{mm}$, $\sigma_B^2 = 1.1530\,\mathrm{mm}^2$
Pavement misalignment	No	256	$\mu_M = -0.1250\,\mathrm{mm}$, $\sigma_M = 1.4857\,\mathrm{mm}$, $\sigma_M^2 = 2.2072\,\mathrm{mm}^2$
Total	Yes	256	All irregularities combined

large sample of already fabricated pavement frames were analysed following the procedure detailed in Refs. [27,37]. A Kolmogorov–Smirnov non-parametric test was used to determine that these two types of unevenness can be statistically characterised as a normal distribution.

Fig. 9 shows a randomly generated unevenness profile for each type of irregularity.

5. Results and analysis

The main results of the research are presented in this section. In order to evaluate the influence of each mode on the dynamic response of the bridges, the cumulative participation of the first 100 modes on the bridge displacement and velocity at mid-span is calculated. On

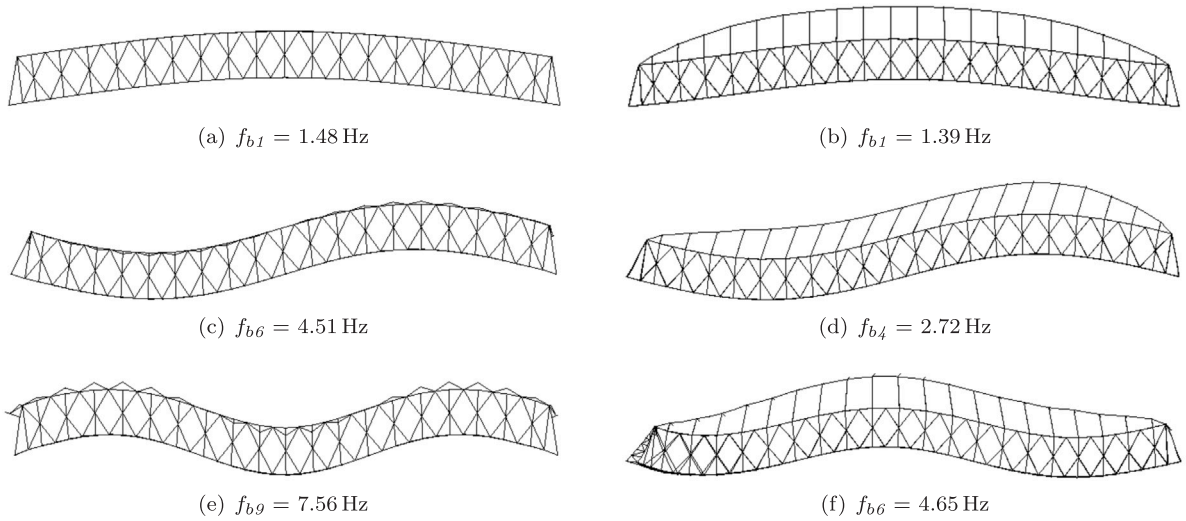

Fig. 8. Longitudinal bending mode shapes of: (a, c, e) the LMB-R120, and (b, d, f) the LMB-A120 bridges.

Table 5
Frequency ranges used to calculate the bridge response using the modal superposition method of the LMB-R and LMB-A bridges.

Bridge	Frequency range	f_b [Hz]
LMB-R120	f_1–f_{22}	[1.47, 13.47]
LMB-R130	f_1–f_{18}	[1.23, 12.06]
LMB-R140	f_1–f_{18}	[1.04, 10.85]
LMB-A120	f_1–f_{14}	[1.39, 7.29]
LMB-A130	f_1–f_{13}	[1.17, 6.46]
LMB-A140	f_1–f_{12}	[0.99, 5.76]

this basis, the frequency range to compute the bridge responses is defined between the fundamental frequency and the fifth longitudinal bending modal frequency of each bridge. Fig. 10 shows the modal Cumulative Contribution in terms of Displacement (DCC) and Velocity (VCC) at mid-span of the LMB-A120 bridge considering a vehicle speed of 90 km/h. The vertical dashed line represents the 14th mode shape, which corresponds to the fifth in-plane bending mode shape. At that point, the modal contribution in the frequency range reaches values greater than 90% for both displacement and velocity. Then, it can be admitted that the frequency range considered is adequate. In the remaining bridges, the same trend is observed. Table 5 lists the selected frequency ranges f_b of all bridges.

The nominal speed considered for the dynamic analyses corresponds to 90 km/h, as it is the maximum design speed allowed in the modular bridges under study. A modal damping ratio $\zeta = 1\,\%$ is set for all the modes according to the AASHTO [24] recommendation for steel structures. As each bridge has two lanes, vehicle passages are simulated with the truck circulating centred in one lane.

5.1. Dynamic forces

In this section, the contact forces produced on the vehicle as a result of the VBI and the bridge acceleration response are studied. Fig. 11 shows the frequency content of the contact force of the front, middle and rear axles of the vehicle considering the quasistatic excitation and the pavement roughness, bowing and misalignment irregularities. The contact force is higher on the middle and rear axles of the truck, which is consistent, as they are located below the rear truck body, which is heavier than the front truck body. In Fig. 11(a), the highest amplitude in the quasistatic contribution is mainly found at low frequencies. The pavement roughness contribution (Fig. 11(b)) is found in the frequency range from 2 to 5 Hz, coinciding with three vertical bouncing modes of the vehicle ($f_{v2} = 2.15$ Hz, $f_{v3} = 3.07$ Hz, $f_{v5} = 4.72$ Hz). Regarding the bowing imperfections in Fig. 11(c), the forces are higher than in the previous cases. A narrow peak is found near 8.93 Hz, which is related to the loading frequency induced by the vehicle $f = v/L_p$, where L_p is the length of the pavement frames and $v = 90$ km/h. In addition, a lower peak appears near 2.23 Hz, approaching the second frequency mode of the vehicle $f_{v2} = 2.15$ Hz. The misalignment irregularity produces the highest contact forces. A notable peak occurs close to 2.08 Hz. Again, this maximum is caused due to the proximity of the second frequency mode of the vehicle, which involves the vertical displacement of the axles and the pitch of the traction and body cars.

Fig. 12 shows the frequency content and the time-history of the total contact force in the front, middle and rear axles of the vehicle considering the combination of the quasistatic and dynamic contributions detailed above. In both cases, the contact force is clearly higher in the middle and rear axles of the truck. Regarding the frequency content, due to the influence of the pavement misalignment, a notable amplification occurs in the proximity of the second frequency mode of the vehicle $f_{v2} = 2.15$ Hz. In the same way, the peak at 8.93 Hz is produced by the effect of bowing imperfections. It can be concluded that these are the two types of irregularities that affect the most the total response.

On the basis of the results from Figs. 11 and 12, it can be deduced that a resonance amplification could occur when the effects of bowing and misalignment are combined. First, the pavement misalignment notably excites the second vertical bouncing frequency of the vehicle ($f_{v2} = 2.15$ Hz), as shown in Fig. 11(d). Then, since the length of the pavement frames is $L_p = 2.8$ m, a resonance speed takes place at $v = 21$ km/h (i.e., 5.83 m/s) because the loading frequency generated at this speed by the bowing irregularities ($f = v/L_p = 5.83/2.8 = 2.08$ Hz) excites the same frequency mode of the vehicle (f_{v2}). Therefore, a notable amplification in the bridge and vehicle responses should be expected when both conditions are met. Next, the dynamic effects at the resonance and the nominal speeds of 21 and 90 km/h are compared.

Fig. 13 presents a comparison of the contact force and acceleration at mid-span for a vehicle travelling at a speed of 90 and 21 km/h. A combination of pavement bowing and misalignment is considered, as they have the highest impact on the total response of the bridge. As can be seen, the amplitude of the contact force at 21 km/h is higher than at 90 km/h, which implies that the contribution of the bowing and misalignment irregularities is also higher at that speed. In Fig. 13(a), the force peaks at 2.15 Hz when $v = 21$ km/h reach maximum values that are much higher than the force at $v = 90$ km/h. Regarding the frequency content of the acceleration in Fig. 13(b), higher accelerations are found

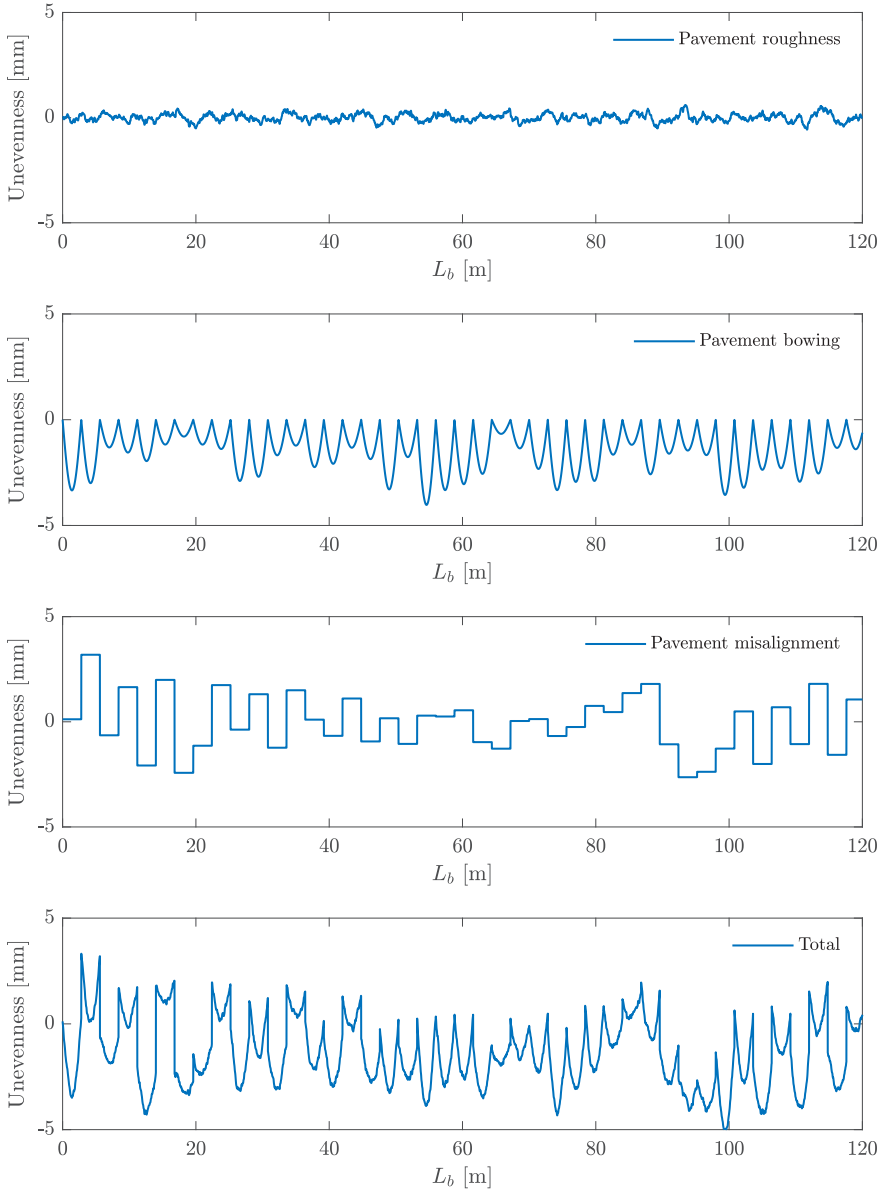

Fig. 9. Randomly generated unevenness profiles of the pavement roughness, bowing, misalignment and total irregularity cases.

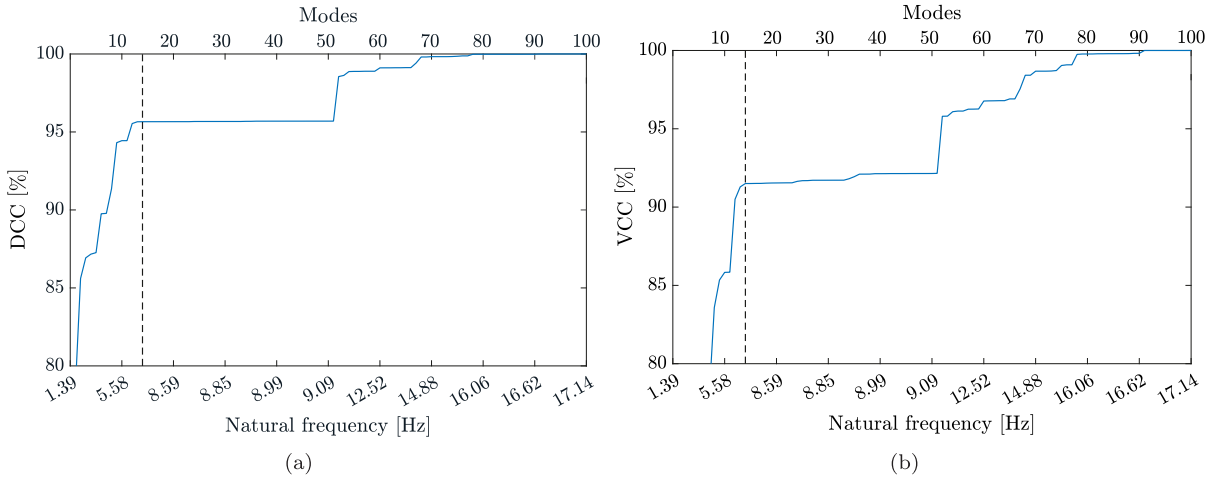

Fig. 10. Cumulative modal contribution for the LMB-A120 bridge in terms of (a) displacement and (b) velocity, at mid-span for a vehicle velocity of 90 km/h and considering all irregularities.

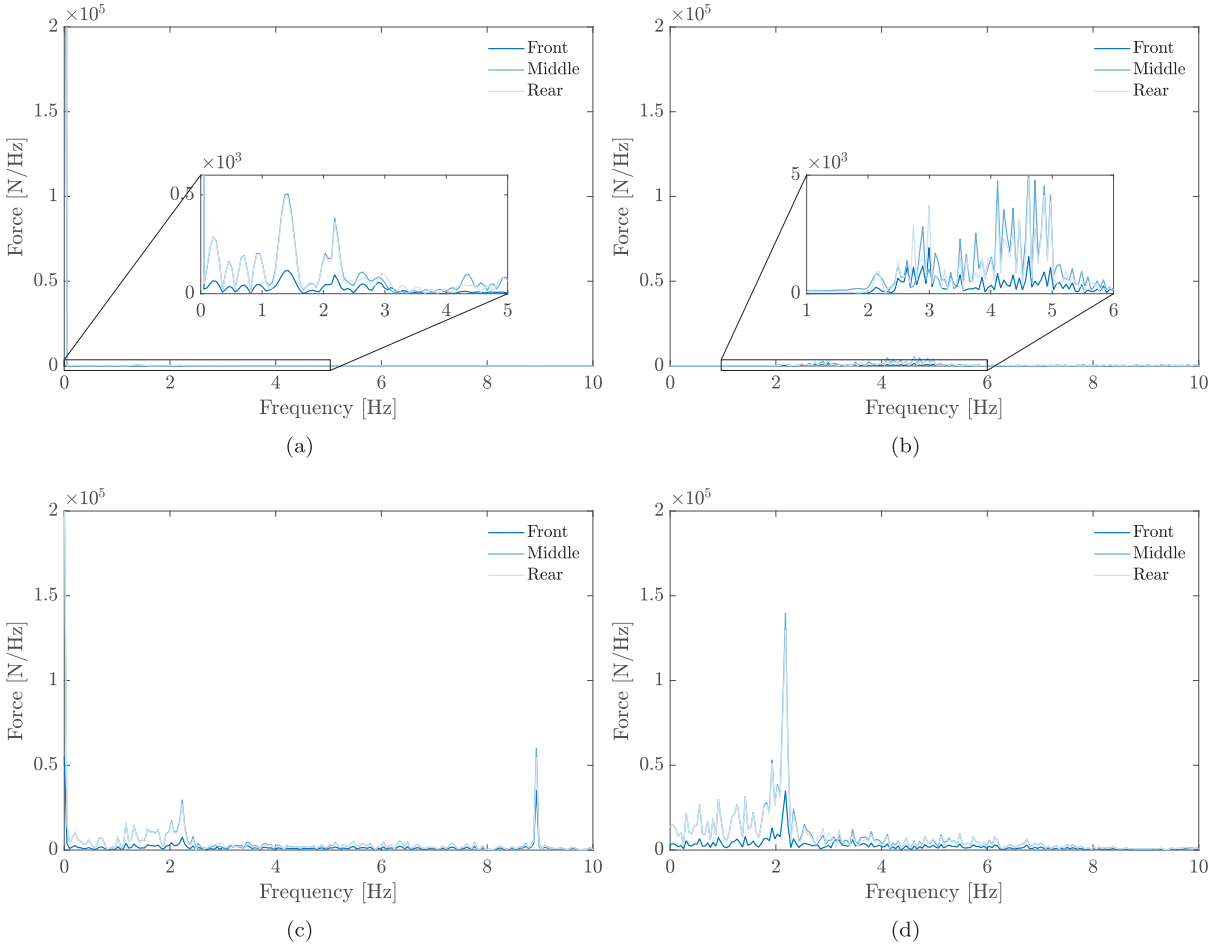

Fig. 11. Frequency content of the contact force at front, middle, and rear axles considering the LMB-A120 bridge and a speed of 90 km/h, for different irregularity cases. (a) Quasistatic; (b) pavement roughness; (c) pavement bowing; and (d) pavement misalignment.

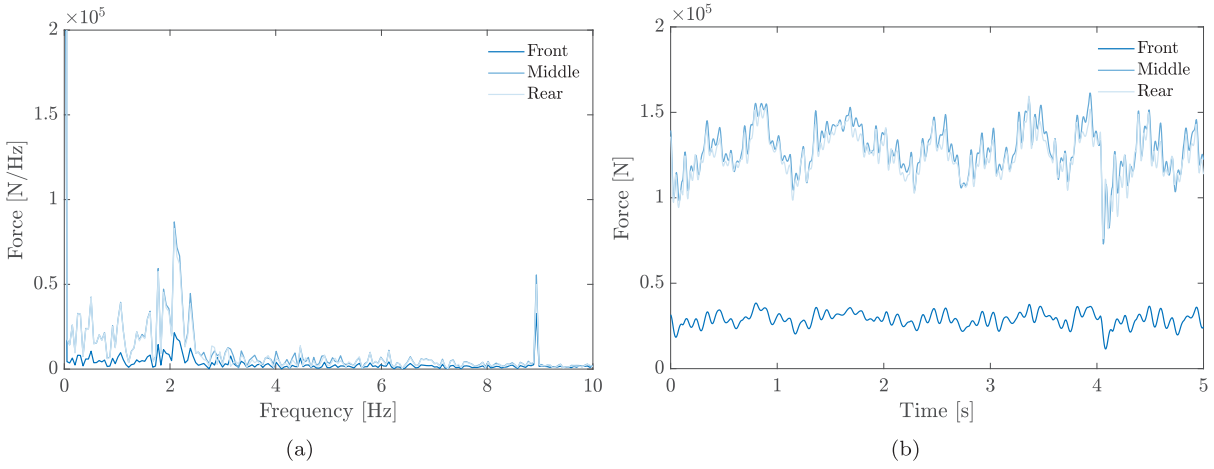

Fig. 12. (a) Frequency content and (b) time history evolution of the total contact force in the LMB-A120 bridge for a travelling speed of 90 km/h.

when $v = 21\,\mathrm{km/h}$. In this case, the highest response occurs close to the fundamental frequency of the bridge $f_{b1} = 1.39\,\mathrm{Hz}$. Another peak is found near the second mode of the vehicle.

A comparison of the acceleration response at mid-span for 90 and 21 km/h considering the total irregularity contribution is presented below. Fig. 14(a) shows the frequency content and 14(b) represents the time-history. As in the previous case, in the resonance speed, peaks appear near the fundamental frequency of the bridge and the second modal frequency of the vehicle. The remaining peaks are minor and are related to higher modes of the structure and the vehicle. In Fig. 14(b), the response at mid-span at $21\,\mathrm{km/h}$ presents higher acceleration levels than at $90\,\mathrm{km/h}$. In particular, a maximum acceleration of $0.36\,\mathrm{m/s^2}$ is

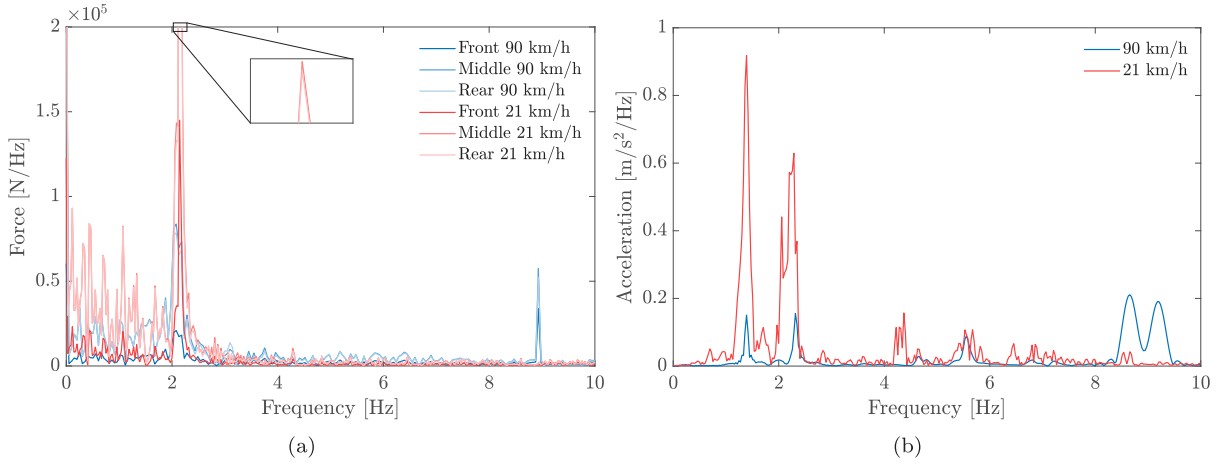

Fig. 13. (a) Frequency content of contact force and (b) LMB-A120 bridge acceleration response at mid-span considering bowing and misalignment contributions and travelling speeds of 90 and 21 km/h.

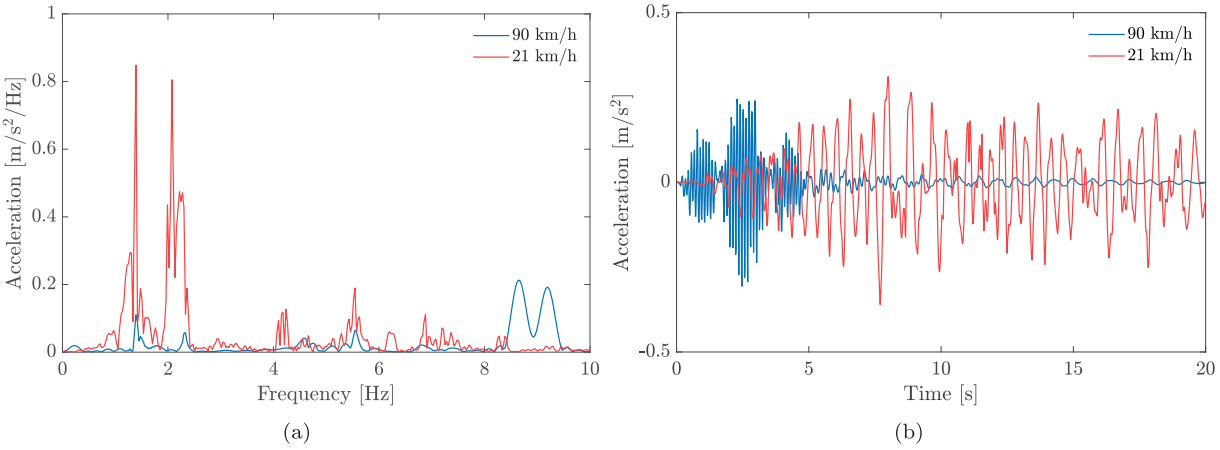

Fig. 14. (a) Frequency content of the total contact force and (b) LMB-A120 bridge acceleration response at mid-span considering the total contribution and travelling speeds of 90 and 21 km/h.

obtained at $t = 7.69$ s. At 90 km/h, the maximum acceleration reached is 0.30 m/s^2 at $t = 2.47$ s.

5.2. Dynamic load allowance

In this section, the dynamic load allowance of the bridges under study is evaluated. To this aim, in the present contribution, IM indices are defined from the average envelopes of the vertical bridge displacement $\overline{u}_b(x)$ after performing S_n simulations:

$$\overline{u}_b(x) = \frac{1}{S_n}\sum_{n=1}^{S_n} \max\left(|u_{bn}(x,t)|\right) \tag{20}$$

Since $\overline{u}_b(x)$ is calculated on a stochastic basis, the standard deviation of the vertical displacement of the bridge at any coordinate x can be expressed as:

$$\sigma_{u_b}(x) = \sqrt{\frac{\sum_{n=1}^{S_n}\left[\max\left(|u_{bn}(x,t)|\right) - \overline{u}_b(x)\right]^2}{S_n}} \tag{21}$$

Furthermore, to ensure that a maximum stable value is obtained, displacement envelopes are also calculated in the 99% percentile (that is, the value of $\overline{u}_b(x)$ that has a probability of being exceeded of less than 1%). In this way, $u_{b\,99\%}(x)$ results in:

$$u_{b\,99\%}(x) = \overline{u}_b(x) + 3\sigma_{u_b}(x) \tag{22}$$

Then, the mean IM indices at each x bridge coordinate are defined as:

$$\overline{IM}(x) = \frac{\overline{u}_b(x)}{u_{b,\,st}(x)} \tag{23}$$

where $u_{b,\,st}(x)$ is the static envelope of the vertical displacement of the bridge. In this case, the static response of the bridge takes into account the self-weight of the vehicle and does not depend on irregularities, so this calculation is performed only once. A maximum statistic value for the IM is defined on the basis of the 99% percentile:

$$IM_{99\%}(x) = \overline{IM}(x) + 3\sigma_{IM}(x) \tag{24a}$$

$$\sigma_{IM}(x) = \frac{\sigma_{u_b}(x)}{u_{b,st}(x)} \tag{24b}$$

where $\sigma_{IM}(x)$ is the standard deviation of the IM indices calculated in all simulations at each x bridge coordinate.

On this basis, Fig. 15(a) shows mean, maximum and static displacement envelopes, while mean and maximum IM indices are shown in 15(b). The parameters are calculated on the LMB-A120 bridge considering the total irregularity contribution for a travelling speed of 90 km/h. As can be seen, in the case of the static load, the maximum displacement takes place in $L_b/2$, whereas in the dynamic one, maximum displacements and IM do not occur at mid-span, but after the vehicle has passed this point. This is caused because of the interlocking effect of the car body on the front and rear wheels described in Ref. [38],

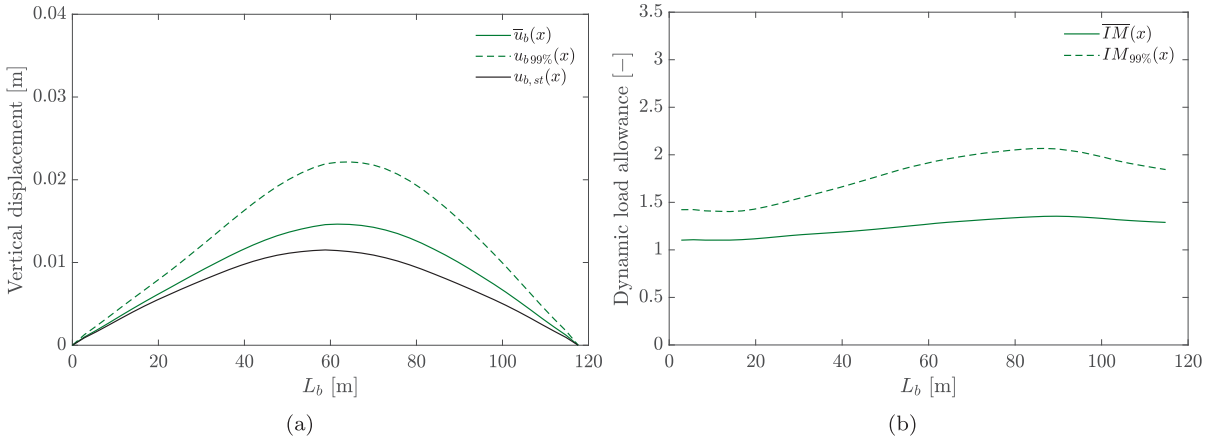

Fig. 15. (a) Envelope of vertical displacement and (b) dynamic load allowance indices of the LMB-A120 bridge for a travelling speed of 90 km/h.

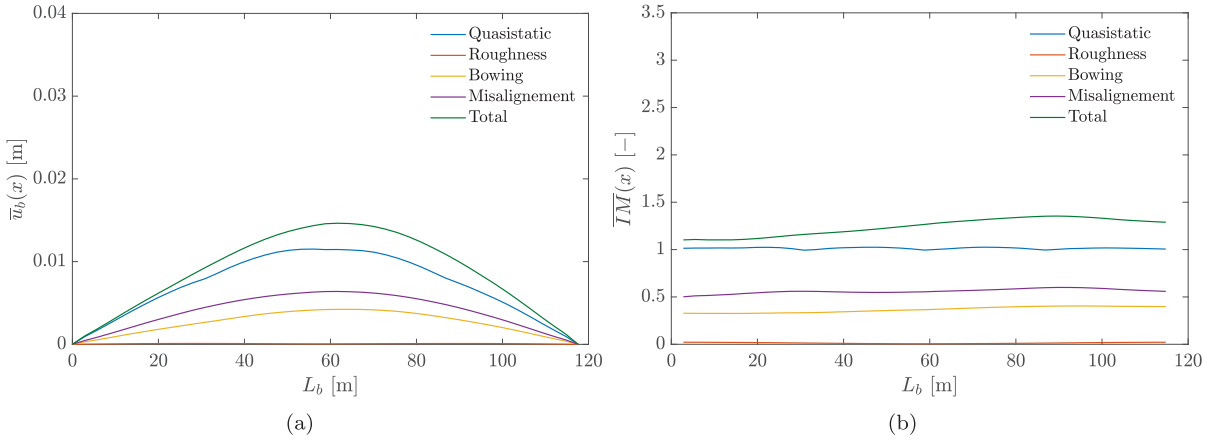

Fig. 16. (a) Envelopes of vertical displacement and (b) mean dynamic load allowance indices for the LMB-A120 bridge for a travelling speed of 90 km/h..

according to which the vehicle gains excitation as it travels through the bridge.

In Fig. 16, the influence of the different load mechanisms on the dynamic load allowance is analysed. The contribution of pavement roughness is negligible. However, it is relevant when it comes to bowing and misalignment. Regarding the IM, a maximum of $\overline{IM} = 1.35$ is reached at $L_b = 90$ m in the total case. The values of IM in the quasistatic contribution are all close to 1 and negligible when it comes to the pavement roughness. In the case of the bowing and misalignment, maximum indices of $\overline{IM} = 0.4$ and $\overline{IM} = 0.6$ are reached at $L_b = 90$ m. Additionally, it should be noted that in both Figs. 16(a) and 16(b), the dynamic amplification obtained from the sum of the quasistatic load and the dynamic contribution due to pavement roughness, bowing and misalignment overestimates the results obtained of the total contribution.

In order to evaluate the dynamic response of the bridges considering road pavements with several levels of deterioration, a sensitivity analysis is performed. Three different road surface conditions accounting for an increasing degree of irregularities are defined and identified as good, medium and poor. The analysis is conducted considering the pavement roughness, bowing and misalignment to assess their independent contribution to the bridge response. Table 6 lists the three road surfaces defined in each case and the corresponding variations applied. In the case of pavement roughness, the good road surface condition corresponds to the nominal case (see Table 4). Medium and poor surfaces are defined according to ISO-8608 [35] and correspond to road classes A and B. In the cases of bowing and misalignment, the good road surface condition matches the nominal configuration in each case,

Table 6
Parametric variations applied on each road surface condition defined in the cases of pavement roughness, bowing and misalignment.

Irregularity type	Road condition	Parameters variation
Pavement roughness	Good	$S(k_0) = 0.35 \times 10^{-6}$ m^3/rad
	Medium	$S(k_0) = 1 \times 10^{-6}$ m^3/rad
	Poor	$S(k_0) = 4 \times 10^{-6}$ m^3/rad
Pavement bowing	Good	$\mu_B = 2.33$ mm, $\sigma_B = 1.07$ mm
	Medium	$\mu_B = 4.66$ mm, $\sigma_B = 2.21$ mm
	Poor	$\mu_B = 9.32$ mm, $\sigma_B = 4.43$ mm
Pavement misalignment	Good	$\mu_M = -0.13$ mm, $\sigma_M = 1.49$ mm
	Medium	$\mu_M = -0.25$ mm, $\sigma_M = 2.97$ mm
	Poor	$\mu_M = -0.50$ mm, $\sigma_M = 5.9$ mm

whereas in the medium and poor surfaces, both the mean and standard deviation of the normal distribution are multiplied by factors of 2 and 4 to increase the average level of unevenness and also its variability.

Fig. 17 shows mean displacement envelopes and IM indices calculated considering different road conditions. The dynamic amplification increases with the deterioration level of the road surface. The IM varies linearly with the parameters shown in Table 4 and the shifts applied to the normal distributions in the bowing and misalignment cases.

Following, the influence of the travelling speed on the dynamic load allowance is evaluated on all the LMB-R and LMB-A bridges. Here, the truck velocity range is extended as: $v = [10, 20, 30, 40, 50, 60, 70, 80, 90, 100, 110]$ km/h. Figs. 18(a) and 18(b) show the mean and maximum IM indices calculated at mid-span for both bridge typologies. The results show that the IM decreases with increasing truck velocities, except

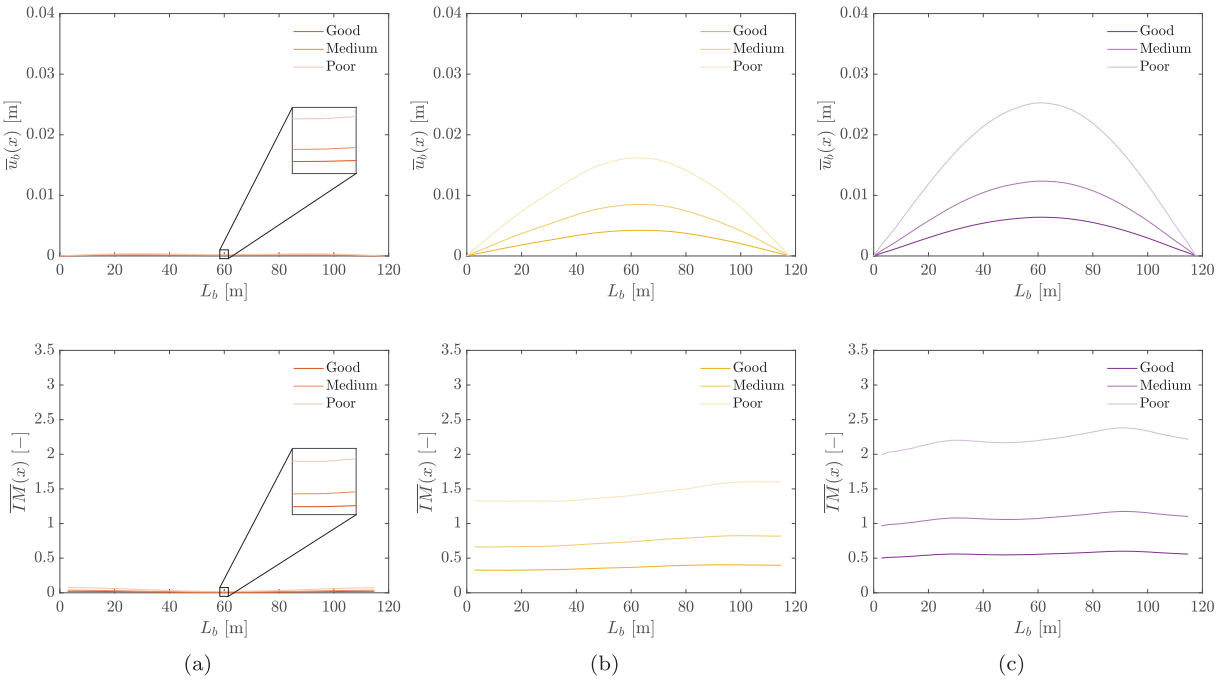

Fig. 17. Dynamic load allowance contribution of (a) the pavement roughness, (b) pavement bowing and (c) pavement misalignment for different road surface condition in the LMB-A120 bridge for a travelling speed of 90 km/h.

when the vehicle approaches a resonance velocity. In relation to the span length, shorter bridges present higher indices for velocities greater than $v = 30$ km/h. Concretely, it is observed that mean IM factors decrease an average of 3.4% for each 10 m extra of span length in non-resonance velocities.

For each typology, regarding the LMB-A bridges, maximum IM indices appear at $v = 20$ km/h due to the proximity of the resonance velocity of 21 km/h. In the particular case of the LMB-A140 bridge, greater values of IM are obtained at $v = 10$ km/h. This effect is produced because the loading frequency induced by the vehicle at that speed matches the fundamental frequency of the bridge $f_{b1} = 0.99$ Hz. A similar response is found in the LMB-R140 bridge, as its fundamental frequency reaches $f_{b1} = 1.04$ Hz. The peak at the resonance speed of $v = 20$ km/h is the highest in the case of the LMB-R130 structure. However, in the LMB-R120 bridge, maximum IM indices are obtained at $v = 30$ km/h. This occurs because the loading frequency associated to that velocity ($f = 2.98$ Hz) matches the first torsional mode of the bridge $f_{b3} = 2.92$ Hz and the third mode of the vehicle ($f_{v3} = 3.07$ Hz), which involves the vertical movement of the masses of the two truck bodies. For the remaining bridges, the first torsional mode, which corresponds to their third frequency mode, takes place at lower frequencies, and thus, this explains why the peak at 30 km/h is only observed in the LMB-R120 bridge. Nonetheless, this implies that the contribution of these modes is more important than the effect of the resonance at 21 km/h in this case. In terms of differences between bridge typologies, the IM is, in general, greater in the LMB-R bridges.

Mean dynamic allowance factors are also determined in terms of internal forces as the ratio between the mean axial deformation in all the simulations and the corresponding deformation in the static case for each bridge element. The total irregularity contribution is considered. Figs. 19 and 20 show mean IM indices of the main structural elements of the bridges considering different truck velocities. The $\overline{IM}$ computed from the displacement data (see Fig. 18) is also represented for comparison purposes. The elements of the reinforced modules are indicated as (R). As can be observed, in general, IM factors decrease as the velocity increases except when approaching a resonance speed in the majority of the bridge structural elements. In this sense, the effect of resonances explained in previous sections is also noticeable in the graphs. However, this is not the case for some bridge components such as the lower chords of the reinforced modules in the LMB-R bridges, where the IM-speed relationship is not clear. An important difference is found between both bridge typologies, since in the LMB-A bridges, vertical elements such as the upper and lower posts and the arch present higher IM factors, whereas, in contrast, in the LMB-R bridges, maximum indices are found in the reinforced lower chords, which are horizontal elements. Thereby, it can be concluded that the presence of the arch may be useful to redistribute internal forces to elements that are not directly subjected to the vehicle, leading to a higher harmonisation of the IM, especially on horizontal structural elements.

6. Discussion

The main findings of the investigation are discussed in this section. In summary, the influence of several parameters such as the road unevenness, the span length and the vehicle speed have been evaluated on the dynamic load allowance of two typologies of LMBs.

To begin with the effect of road irregularities, the results of this work draw a clear relation between poorer road surface conditions and higher levels of IM (see Fig. 17). This trend is in agreement with a good number of publications and studies that have come with similar conclusions [20–22,28,31]. In this sense, it is important to remark that in the bridges under study, the greatest contribution to the total bridge response is caused by bowing and misalignment defects, as they excite the vertical bouncing modes of the vehicle and, therefore induce a higher response on the structure. Other authors [15,39] also identified the bouncing of the truck load as a primary source of bridge excitation that contributed to the obtaining of higher IM indices.

Apart from the road unevenness, there are multiple aspects involving VBI that affect the dynamic load allowance of a bridge. Among them, the span length is a factor whose influence remains uncertain. As cited in [31], several studies have been carried out on this matter in a variety of bridges with no concluding agreement. The results obtained in this paper reported in Fig. 18 point to a minor influence of the span length on LMBs, leading to an average 3.4% decrease of the IM per every 10 m extra of span length of the two typologies considered in

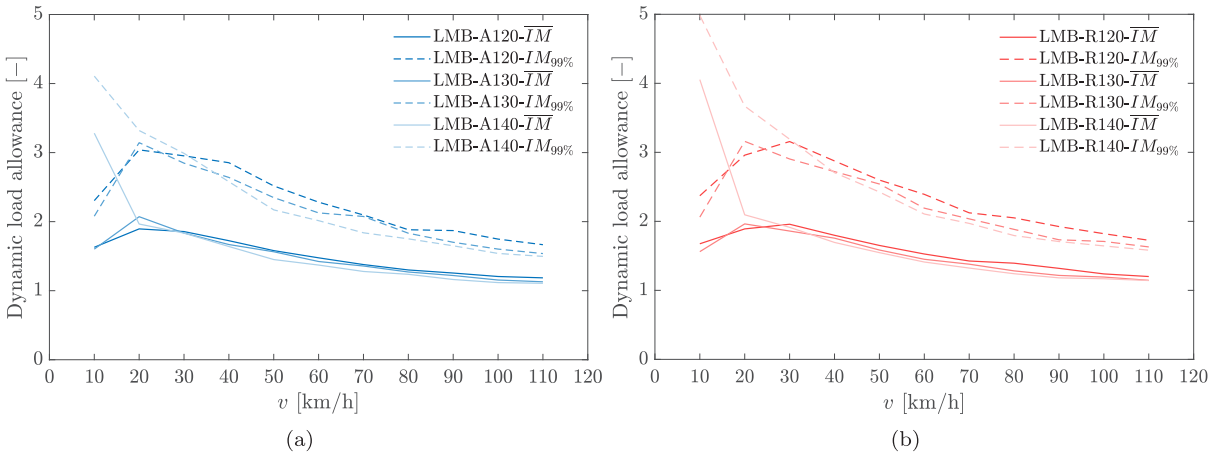

Fig. 18. Influence of the travelling speed on the dynamic load allowance at the mid-span of (a) LMB-A and (b) LMB-R bridges.

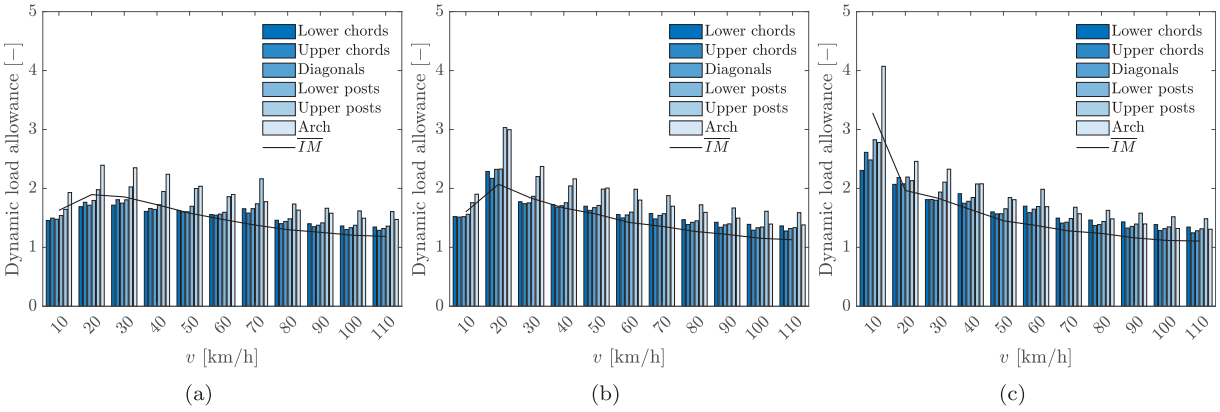

Fig. 19. Influence of the travelling speed on the dynamic load allowance calculated in terms of internal element forces of (a) LMB-A120, (b) LMB-A130 and (c) LMB-A140 bridges.

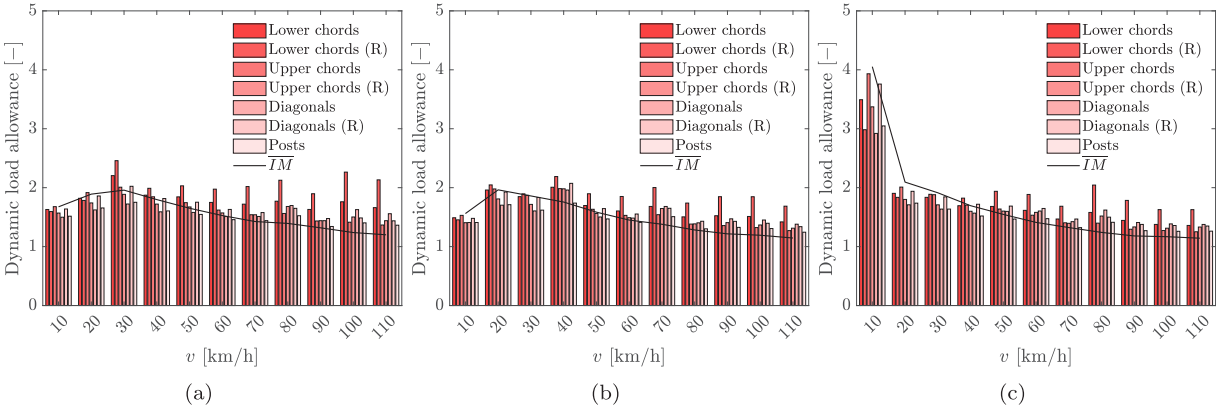

Fig. 20. Influence of the travelling speed on the dynamic load allowance calculated in terms of internal element forces (a) LMB-R120, (b) LMB-R130 and (c) LMB-R140 bridges.

non-resonance velocities. Similar trends are found in Refs. [4,40] for concrete bridges. However, in those cases, divergences between span lengths and the IM are more accentuated. One of the reasons that may explain the small variations found in the present contribution are the large spans considered, as in [4], differences in IM indices between span lengths are less pronounced in larger bridges. In this way, structures with longer spans could have a higher capacity to dissipate the energy impelled by a vehicle.

Another key factor which is thought to have an important influence on the IM is the vehicle speed. However, the relationship between both parameters is rather controversial, as previous research has yielded to inconsistent findings [31,41,42]. Indeed, several studies have concluded that the effect of the speed on the IM is influenced by other factors such as the vehicle weight, road roughness, span length, etc. [31], accentuating the difficulty of obtaining clear conclusions. In the present investigation, as derived from the results from Figs. 18–20, IM indices tend generally to decrease as the velocity increases, except when resonance is produced. This effect could be caused because at high velocity, and taking into account the large span of the bridges considered, there may be not enough time for the force to compel a significant dynamic deflection on the bridge [26]. Nevertheless, IM indices calculated on the basis of the internal forces of some bridge

Table 7
IM indices obtained at 21 and 90 km/h from the displacement $\overline{IM}_u$ and internal forces $\overline{IM}_F$, compared to those calculated based on several design codes.

Bridge	$\overline{IM}_{u21}$	$\overline{IM}_{F21}$	$\overline{IM}_{u90}$	$\overline{IM}_{F90}$	AASHTO	EC1	NBR-7188	CSA	BS5400-2
LMB-A120	1.86	1.89	1.26	1.44	1.33	1.16	1.13	1.25	1.25
LMB-A130	2.07	2.52	1.22	1.43	1.33	1.14	1.12	1.22	1.25
LMB-A140	1.97	2.19	1.16	1.41	1.33	1.11	1.11	1.20	1.25
LMB-R120	1.89	1.59	1.32	1.51	1.33	1.16	1.12	1.26	1.25
LMB-R130	1.96	1.88	1.21	1.49	1.33	1.14	1.12	1.23	1.25
LMB-R140	2.09	1.77	1.18	1.41	1.33	1.11	1.11	1.21	1.25

elements present an ambiguous IM-speed relation (see lower reinforced chords on Fig. 20). In a similar way, results for the complete structure reported in Refs. [4,43] also depict an unclear relation between both parameters. With regard to studies on modular bridges, Refs. [27,28] find increasing IM with higher speeds. However, in these works, the bridges considered have a span length which is significantly shorter (39 and 60 m), the truss section is smaller and it is spatially distributed in a different manner with only one connection between both sides of each module. These reasons may explain the different outcomes obtained in comparison with the present paper. In any case, as can be seen, the IM-speed relation is complex and does not follow a simple tendency [23]. Further analysis is still required in this regard.

Finally, it is also interesting to compare the IM indices obtained with those provided by various design codes, as they do not take into account the road roughness or the velocity of the vehicle associated with a potential resonant effect [44]. In fact, although some design codes implicitly consider dynamic amplification, others define the IM based on single factors or derived from the bridge span length [4,23]. Table 7 compares, for the bridges under study, the IM indices obtained from the dynamic analyses and those calculated on the basis of the empirical formulas given in the following design codes: AASHTO [24], EC1 [45], NBR-7188 [46], CSA [47] and BS5400-2 [48]. Numerical IM indices are calculated at 21 and 90 km/h considering the total irregularity contribution. In this section, $\overline{IM}_u$ refers to the mean IM indices calculated from the bridge displacement and $\overline{IM}_F$ indicates those calculated in terms of the internal forces of the bridge elements. In this case, $\overline{IM}_F$ is the mean of the indices obtained for the elements listed in Figs. 19 and 20.

For a better understanding of the results, Fig. 21 summarises the content of Table 7. As can be seen, IM indices obtained between all the design codes considered are similar. Additionally, the ones calculated at 90 km/h are closer to the standards. In this regard, indices provided by AASHTO [24] are the most conservative and are sufficient compared to $\overline{IM}_{u90}$. However, these values are slightly exceeded when compared to $\overline{IM}_{F90}$. The same trend is observed with respect to the CSA [47] and BS5400-2 [48] standards, with the exception of the LMB-A120 and LMB-R120 bridges. Indices provided by EC1 [45] and NBR-7188 [46] underestimate the response of all structures. In any case, the highest divergences are given when considering a resonance situation ($v = 21$ km/h), at which the values of dynamic load allowance increase. In this case, the differences from the standards are more pronounced.

7. Conclusions

In this contribution, the dynamic load allowance of two typologies of long-span modular steel bridges is evaluated. For this purpose, a 3D vehicle–bridge interaction model is implemented. Three bridges with increasing span lengths are studied for each typology and modelled by means of the FEM. The vehicle is a HS20-44 truck defined in AASHTO [24]. It is assumed that the presence of the vehicle does not alter the properties of the bridge and thus the modal superposition method is used to calculate the response of the bridge. The effect of different types of randomly-generated road irregularities is simulated on the bridge decks. The VBI is studied through the contact forces that appear on the axles of the vehicle. Also, the bridge acceleration at mid-span is evaluated under several irregularity types and velocities. Then, displacement envelopes and IM indices are compared considering different irregularity cases, span lengths and vehicle speeds. The main conclusions regarding the VBI and the dynamic load allowance of the LMBs under study are as follows.

- With respect to the contact forces on the axles of the vehicle, the greatest force amplification occurs when considering the misalignment of the pavement. This type of irregularity, consisting of a vertical step defect on the road surface, excites the second mode of the vehicle, which involves the vertical movement of the front and rear body trucks. Other defects such as the pavement bowing also derive in a relevant force amplification. In this case, the bowing effect depends on the characteristic length of the pavement, which produces a specific amplification on the loading frequency associated with this length. Because of this, an important amplification of the contact force occurs at $v = 21$ km/h as the second mode of the vehicle is also excited by the bowing defects. In sum, these irregularity types are the ones that affect the most the response of the bridges. The effect of other irregularities, such as the pavement roughness is less relevant.
- It is observed that there exist multiple conditions that can lead to resonance as both the vehicle and the bridge have different natural frequencies. This should be taken into account when designing LMBs, as the vehicle travelling at resonance velocity (which can be relatively low) may induce an important response of the bridge in terms of acceleration and displacement. Since resonance effects may also be related to defects on the bridge deck, this circumstance should also be considered.
- The highest values of dynamic load allowance are reached when all irregularities are combined. Furthermore, the IM increases as the condition of the road surface deteriorates.
- The effect of increasing the span length on LMBs is found to cause a slight reduction on the IM in non-resonance velocities.
- In the LMBs under study, the IM tends, in general, to decrease as the velocity increases, except when resonance is produced. Nevertheless, it is observed that in the particular case of certain elements such as the reinforced lower chords of the LMB-R bridges, the IM follows no clear relation with the speed.
- In what concerns the dynamic performance of both typologies, LMB-R bridges present higher IM. The truss configuration is found to be relevant in order to redistribute the bridge stresses, having a clear influence on the resulting IM indices of each bridge element. Regarding the LMB-A typology, the arch is the structural element that exhibits higher IM indices, especially in the case of the shortest bridges LMB-A120 and LMB-A130, and at the lowest speeds. In this sense, the arch is useful to redistribute internal forces to elements that are not directly subjected to the vehicle. However, in the LMB-R bridges, higher internal forces are found on horizontal structural members such as the lower chords.
- Finally, the results obtained highlight some inconsistencies between the IM indices calculated and those predicted with the expressions available in the structural standards. At a speed of 90 km/h, due to the large size of the span length, some design codes underestimate the response of the bridge. In this regard,

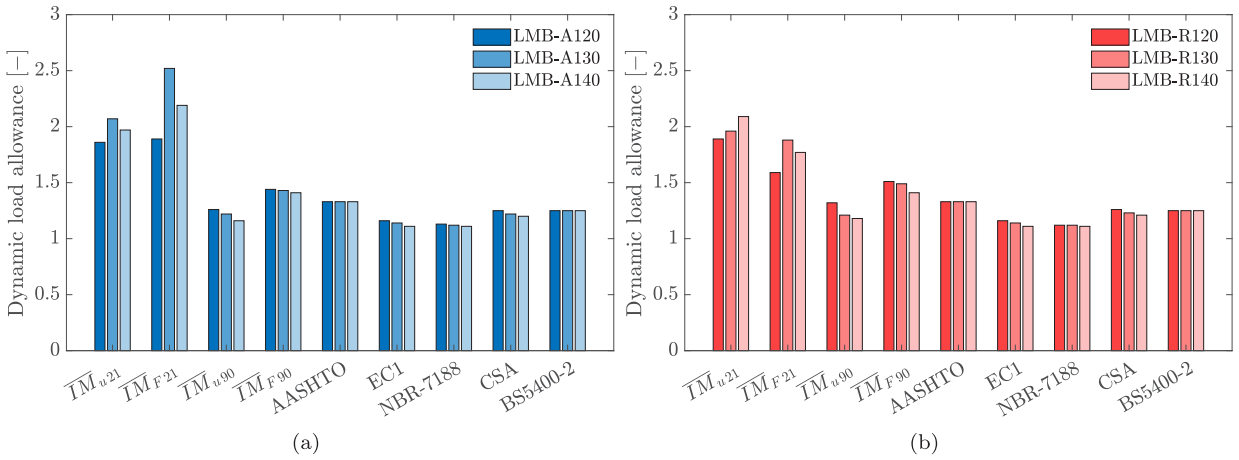

Fig. 21. Comparison of the IM indices calculated from the dynamic analyses and on the basis of several design codes for the (a) LMB-A and (b) LMB-R bridges.

AASHTO [24] provides suitable IM values for the LMBs, but at resonance, IM indices increase and the values given by AASHTO [24] are exceeded. In summary, the main reasons for these divergences are (i) the lack of adaptability to the type of bridge of the formulas given in the design codes (in this case, to the long-span modular bridges) and (ii) the fact that resonance and road deterioration are not considered in those expressions.

This investigation explores the VBI phenomenon and the dynamic load allowance of long-span modular steel bridges, which is a key aspect in order to develop this technology and to build larger, better and safer structures. In this work, conclusions are drawn from the study of two bridge typologies that represent two different approaches based on the concept of modular construction. However, future investigations are still required to fully understand the dynamic effects of these structures to overcome their limitations and enhance their potential on the global transportation infrastructure.

CRediT authorship contribution statement

J. Chordà-Monsonís: Conceptualization, Methodology, Software, Validation, Formal analysis, Writing – original draft, Writing – review & editing. **E. Moliner:** Formal analysis, Writing – original draft, Writing – review & editing. **P. Galvín:** Conceptualization, Methodology, Formal analysis, Writing – original draft, Writing – review & editing, Funding acquisition. **M.D. Martínez-Rodrigo:** Formal analysis, Writing – original draft, Writing – review & editing, Funding acquisition. **E. Zacchei:** Formal analysis, Writing – original draft, Writing – review & editing. **A. Tadeu:** Conceptualization, Funding acquisition. **I. Ferraz:** Conceptualization. **A. Romero:** Conceptualization, Methodology, Software, Validation, Formal analysis, Writing – original draft, Writing – review & editing, Supervision, Funding acquisition.

Declaration of competing interest

The authors declare that they have no known competing financial interests or personal relationships that could have appeared to influence the work reported in this paper.

Data availability

Data will be made available on request.

Acknowledgements

The authors would like to acknowledge the financial support provided by the Spanish Ministry of Science and Innovation under the research project PID2019-109622RB; Generalitat Valenciana, Spain under the research project AICO/2021/200; Junta de Andalucía, Spain and the European Social Fund through the contract USE-22311-R with the Universidad de Sevilla and the Andalusian Scientific Computing Centre (CICA), Spain. This work was also carried out under POCI-01-0247-FEDER-039742 (SELF-Bridges-Long-Span Modular Bridges: Smarter, Extensible, Lighter and Fast Assembly). Project funded by Portugal through COMPETE 2020.

References

[1] Kim CW, Kawatani M, Kim KP. Three-dimensional dynamic analysis for bridge–vehicle interaction with roadway roughness. Comput Struct 2005;83:1627–45.
[2] Li H, Wang T, Wu G. A Bayesian deep learning approach for random vibration analysis of bridges subjected to vehicle dynamic interaction. Mech Syst Signal Process 2022;170:108799.
[3] Shi Z, Uddin N. Theoretical vehicle bridge interaction model for bridges with non-simply supported boundary conditions. Eng Struct 2021;232:111839.
[4] Deng L, Cai S. Development of dynamic impact factor for performance evaluation of existing multi-girder concrete bridges. Eng Struct 2010;32:21–31.
[5] Wang Y, Thrall AP, Zoli TP. Adjustable module for variable depth steel arch bridges. J Construct Steel Res 2016;126:163–73.
[6] Kusimba B, Rinzin T, Banno Y, Kinoshita K. Condition assessment and adaptation of bailey bridges as a permanent structure. Appl Sci 2022;12:22:137–46.
[7] André A, Fernandes J, Ferraz I, Pacheco P. New modular bridges solutions. In: 9th International symposium on steel bridges, vol. 419. 2018, 012021.
[8] Huile L, Wang T, Gang W. A Bayesian deep learning approach for random vibration analysis of bridges subjected to vehicle dynamic interaction. Mech Syst Signal Process 2022;170:108799.
[9] Yang YB, Lin CW. Vehicle–bridge interaction dynamics and potential applications. J Sound Vib 2005;284:205–26.
[10] Chul WK, Kawatani M, Ki BK. Three-dimensional dynamic analysis for bridge–vehicle interaction with roadway roughness. Comput Struct 2005;83:1627–45.
[11] Liu K, De Roeck G, Lombaert G. The effect of dynamic train–bridge interaction on the bridge response during a train passage. J Sound Vib 2009;325:240–51.
[12] Yang YB, Zhang B, Wang T, Xu H, Wu Y. Two-axle test vehicle for bridges: Theory and applications. Int J Mech Sci 2019;152:51–62.
[13] Greco F, Lonetti P. Numerical formulation based on moving mesh method for vehicle–bridge interaction. Adv Eng Softw 2018;121:75–83.
[14] Cantero D, McGetrick P, Kim C, OBrien E. Experimental monitoring of bridge frequency evolution during the passage of vehicles with different suspension properties. Eng Struct 2019;187:209–19.
[15] Junhee K, Jerome PL. Experimental analysis of vehicle–bridge interaction using a wireless monitoring system and a two-stage system identification technique. Mech Syst Signal Process 2012;28:3–19.
[16] Matsuoka K, Kaito K, Sogabe M. Bayesian time–frequency analysis of the vehicle–bridge dynamic interaction effect on simple-supported resonant railway bridges. Mech Syst Signal Process 2020;135:106373.

[17] Galvín P, Domínguez J. Dynamic analysis of a cable-stayed deck steel arch bridge. J Construct Steel Res 2007;63(8):1024–35.
[18] Stoura D, Dimitrakopoulos E. Additional damping effect on bridges because of vehicle-bridge interaction. J Sound Vib 2020;476:115294.
[19] Yau JD, Martínez-Rodrigo MD, Doménech A. An equivalent additional damping approach to assess vehicle-bridge interaction for train-induced vibration of short-span railway bridges. Eng Struct 2019;188:469–79.
[20] Oliva J, Gociolea JM, Antolín P, Astiz Má. Relevance of a complete road surface description in vehicle–bridge interaction dynamics. Eng Struct 2013;56:466–76.
[21] Camara A, Nguyen K, Ruiz-Teran AM, Stafford PJ. Serviceability limit state of vibrations in under-deck cable-stayed bridges accounting for vehicle-structure interaction. Eng Struct 2014;61:61–72.
[22] Bhetuwal U, Shrestha JK, Pradhananga R. Fatigue life analysis of steel–concrete composite bridge considering road surface conditions. Innov Infrastruct Solut 2022;7(124).
[23] Ma L, Zhang W, Han WS, Liu JX. Determining the dynamic amplification factor of multi-span continuous box girder bridges in highways using vehicle-bridge interaction analyses. Eng Struct 2019;181:47–59.
[24] AASHTO. American Association of State Highway and Transportation Officials. LFRD Bridge Design Specifications. techreport, 2017.
[25] Jung H, Kim G, Park C. Impact factors of bridges based on natural frequency for various superstructure types. J Civ Eng 2013;17(2):458–64.
[26] Mohseni I, Khalim AR, Nikbakht E. Effectiveness of skewness on dynamic impact factor of concrete multicell box-girder bridges subjected to truck loads. Arab J Sci Eng 2014;39:6083–97.
[27] Montenegro PA, Castro JM, Calçada R, Soares JM, Coelho H, Pacheco P. Probabilistic numerical evaluation of dynamic load allowance factors in steel modular bridges using a vehicle-bridge interaction model. Eng Struct 2021;226:111316.
[28] Pinkney B, Dagenais MA, Wight G. Dynamic load testing of a modular truss bridge using military vehicles. Eng Struct 2022;254:113822.
[29] Svendsen BT, Frøseth TG, Rönnquist A. Damage detection applied to a full-scale steel bridge using temporal moments. Shock Vib 2020;3083752.
[30] Mousavi AA, Zhang C, Masri FS, Gholipour G. Structural damage localization and quantification based on a ceemdan Hilbert transform neural network approach: A model steel truss bridge case study. Sensors 2020;20(5):1271.
[31] Deng L, Yang Y, Zou Q, Cai CS. State-of-the-art review of dynamic impact factors of highway bridges. J Bridge Eng 2015;20:04014080.
[32] Henchi K, Fafard M, Talbot M, Dhatt G. An efficient algorithm for dynamic analysis of bridges under moving vehicles using a coupled modal and physical components approach. J Sound Vib 1998;212(4):663–83.
[33] Dormand J, Prince P. A family of embedded Runge-Kutta formulae. J Comput Appl Math 1980;6(1):19–26.
[34] Shampine L, Reichelt M. The MATLAB Code Suite. SIAM J Sci Comput 1997;18(1):1–22.
[35] International Organization for Standardization (ISO), mechanical vibration - road surface profiles - reporting of measured data, ISO-8608:2016, Geneva, Switzerland, p. 44, 2016. Techreport, 2016.
[36] BERD. Bridge Engineering Research and Design, Portugal. Techreport, 2019, (Accessed July 2019).
[37] Calçada R, Montenegro P, Castro M. Numerical evaluation of the dynamic load allowance factor im from ASHTOO in steel modular bridges from the Peru Provias Project: probabilistic approach. Techreport, 2019.
[38] Yang YB, Yau J, Wu YS. Vehicle-bridge interaction dynamics with applications to high-speed railways. 2004.
[39] Kwasniewski L, Wekezer J, Roufa G, Li H, Ducher J, Malachowski J. Experimental evaluation of dynamic effects for a selected highway bridge. J Perform Construct Facilities 2006;20:253–60.
[40] Li H. Dynamic response of highway bridges subjected to heavy vehicles (Ph.D. Thesis), Dept. of Civil and Environmental Engineering, Florida State Univ., Tallahassee, FL.; 2008.
[41] Ashebo B, Chan H, Yu L. Evaluation of dynamic loads on a skew box girder continuous bridge part II: Parametric study and dynamic load factor. Eng Struct 2006;29:1064–73.
[42] Broquet C, Bailey F, Fafard M, Brühwiler E. Dynamic behavior of deck slabs of concrete road bridges. J Bridge Eng 2004;9:2:137–46.
[43] Shi X. Structural performance of approach slab and its effect on vehicle induced bridge dynamic response (LSU Doctoral Dissertations), 2006.
[44] Liu K, Zhou H, Shi G, Wang YQ, Shi YJ, De Roeck G. Fatigue assessment of a composite railway bridge for high speed trains. part II: Conditions for which a dynamic analysis is needed. J Construct Steel Res 2013;82:246–54.
[45] CEN. Action on structures - Part 2: traffic loads on bridges, in: EN 1991-2, European Committee for Standardization, Brussels. Techreport, 2002.
[46] Associação Brasileira de Normas Técnicas (ABNT), Norma Brasileira NBR 7188, Carga móvel rodoviária e de pedestres em pontes, viadutos, passarelas e outras estruturas. Techreport, 2013.
[47] Canadian Standard Association (CSA) S6:19, Canadian Highway Bridge Design Code. techreport, 1974.
[48] British Standards Institution (BSI), BS5400-2 Steel, concrete and composite bridges. Techreport, 2006.